



Published in final edited form as:

Cell Rep. 2022 March 29; 38(13): 110572. doi:10.1016/j.celrep.2022.110572.

Microbes affect gut epithelial cell composition through immune-dependent regulation of intestinal stem cell differentiation

Xi Liu^{1,2,6}, Peter Nagy^{1,6}, Alessandro Bonfini¹, Philip Houtz^{1,3}, Xiao-Li Bing^{1,4}, Xiaowei Yang^{1,5}, Nicolas Buchon^{1,7,*}

¹Cornell Institute of Host-Microbe Interactions and Disease, Department of Entomology, Cornell University, 129 Garden Avenue, Ithaca, NY 14853, USA

²Present address: Instrumental Analysis Center, Shanghai Jiao Tong University, 800 Dongchuan Road, Shanghai 200240, China

³Present address: Department of Biomedical Engineering, Tufts University, 419 Boston Avenue, Medford, MA 02155, USA

⁴Present address: Department of Entomology, Nanjing Agricultural University, Nanjing 210095, China

⁵Present address: State Key Laboratory for Biology of Plant Diseases and Insect Pests, Institute for Plant Protection, Chinese Academy of Agricultural Sciences, Beijing 100193, China

⁶These authors contributed equally

⁷Lead contact

SUMMARY

Gut microbes play important roles in host physiology; however, the mechanisms underlying their impact remain poorly characterized. Here, we demonstrate that microbes not only influence gut physiology but also alter its epithelial composition. The microbiota and pathogens both influence intestinal stem cell (ISC) differentiation. Intriguingly, while the microbiota promotes ISC differentiation into enterocytes (EC), pathogens stimulate enteroendocrine cell (EE) fate and long-term accumulation of EEs in the midgut epithelium. Importantly, the evolutionarily conserved *Drosophila* NFκB (Relish) pushes stem cell lineage specification toward ECs by directly regulating differentiation factors. Conversely, the JAK-STAT pathway promotes EE fate in response to infectious damage. We propose a model in which the balance of microbial pattern

This is an open access article under the CC BY-NC-ND license (<http://creativecommons.org/licenses/by-nc-nd/4.0/>).

*Correspondence: nicolas.buchon@cornell.edu.

AUTHOR CONTRIBUTIONS

Conceptualization, X.L., P.N., and N.B.; methodology and investigation, X.L., P.N., A.B., P.H., X.-L.B., and X.Y.; software, X.-L.B. and X.Y.; formal analysis, X.L., P.N., X.-L.B., X.Y., and N.B.; writing – original & review and visualization, X.L., P.N., and N.B.; validation, resources, project administration, funding acquisition, and supervision, N.B.

DECLARATION OF INTERESTS

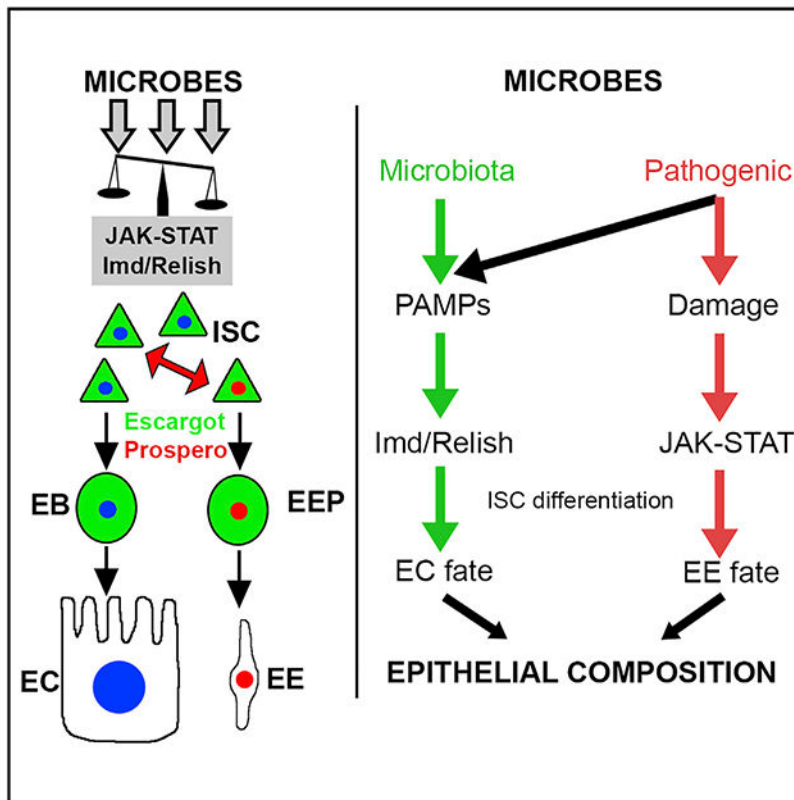
The authors declare no competing interests.

SUPPLEMENTAL INFORMATION

Supplemental information can be found online at <https://doi.org/10.1016/j.celrep.2022.110572>.

recognition pathways, such as Imd-Relish, and damage response pathways, such as JAK-STAT, influence ISC differentiation, epithelial composition, and gut physiology.

Graphical Abstract



In brief

Liu et al. find that gut microbes impact intestinal stem cell differentiation, thus changing epithelial composition. All microbes stimulate the Imd/Relish pathway (NF- κ B), but pathogens additionally generate stress and damage that stimulate the JAK-STAT pathway, leading to accumulation of enteroendocrine cells.

INTRODUCTION

The gut is the primary interface between microbes and their host (Miguel-Aliaga et al., 2018). Substantial evidence indicates that intestinal stem cells (ISCs) play a pivotal role in maintaining gut integrity and adjusting its structure in response to luminal content, but they also play a role in initiating cancer development (Miguel-Aliaga et al., 2018; Radtke and Clevers, 2005). Changes in the microbial, chemical, and nutritional content of the lumen have been shown to alter ISC activity and reshape gut structure and function (Buchon et al., 2009a, 2009b; O'Brien et al., 2011; Peck et al., 2017). However, an understanding of the mechanisms by which gut microbes influence gut homeostasis and host physiology remain

insufficient, and a complete understanding of the molecular dialogue between the host and its microbiome is still lacking.

Conserved microbial patterns mediate the induction of immune responses in vertebrates and *Drosophila* (Akira et al., 2006; Hultmark, 2003). First, microbe-derived molecules called pathogen-associated molecular patterns (PAMPs) can be detected and stimulate immune pathways such as the Toll and Imd-Relish pathways (Buchon et al., 2014). In addition, exposure to pathogens or epithelial damage can trigger immune activation by stimulating the JAK-STAT pathway (Buchon et al., 2009b; Richmond et al., 2018). The *Drosophila* immune response is activated downstream of detecting microbe-derived molecules (e.g., peptidoglycan [PGN] or Muramyl-Di-Peptide) and epithelial damage secondary to bacterial virulence (Houtz et al., 2017). Intestinal inflammation provoked by deregulated immune activation increases the risk of cancer development, suggesting that these conditions are connected (Bernstein et al., 2001; Dyson and Rutter, 2012) and that immune activation in the gut (e.g., inflammatory signals) regulates ISC proliferation (Buchon et al., 2009a).

In *Drosophila*, two differentiated cell types coexist in the midgut epithelium (Figure S1A): absorptive enterocytes (ECs) represent 90% of differentiated cells, while secretory enteroendocrine cells (EEs) represent only 10% (Biteau and Jasper, 2014). As in mammals, differentiated cell types are maintained by the controlled activity of progenitor cells via highly conserved signaling pathways (Apidianakis and Rahme, 2011; Liu et al., 2017). In *Drosophila*, progenitors (expressing the transcription factor *Escargot* or *Esg*), including pluripotent ISCs, committed EC precursors called enteroblasts (EBs), and EE precursors (EEPs). ISCs oscillate between two states and produce terminally differentiated cell types: (1) differentiating ISCs that transiently express the transcription factor *prospero* (*pros*) give rise to EEPs and, ultimately, EEs (Chen et al., 2018), and (2) differentiating ISCs that do not express *pros* give rise to EBs and, ultimately, ECs (Biteau and Jasper, 2014; Zeng and Hou, 2015). ISC differentiation into ECs is determined by the interplay of multiple signaling pathways including the Notch (Micchelli and Perrimon, 2006; Ohlstein and Spradling, 2007) and Dpp/TGF β (Zhou et al., 2015) pathways. The transcription factor Sox21a is also a major determinant of EC fate, among others (Chen et al., 2016; Zhai et al., 2015, 2017). Both pathogenic infection and dysbiosis trigger dynamic remodeling of the *Drosophila* gut coupled with an accelerated rate of epithelium turnover (Buchon et al., 2009a; Jiang et al., 2009; Ryu et al., 2008). This remodeling coordinates the elimination of damaged cells, notably ECs, with the synthesis of new epithelial cells (Buchon et al., 2009b, 2010; Jiang et al., 2009). As a consequence, the presence of bacteria stimulates ISC division, which is essential for repairing infection-induced tissue damage (Houtz et al., 2017).

In this study, we aim to characterize key signals and pathways that mediate the molecular dialogue between a host and its gut microbes. Our analysis of intestinal epithelial cell composition by microscopy revealed that the gut microbiota and pathogens promote opposing changes to gut structure by altering the relative proportion of terminally differentiated ECs and EEs. Specifically, the microbiota promoted formation of ECs while ingestion of pathogens stimulated an increase in EEs, demonstrating different microbial effects on ISC activity. To further elucidate this differential impact of the microbiota and pathogens, we applied complementary genomic approaches to characterize the influence of

pathogenic/non-pathogenic microbes on two immune pathways: the NF κ B and JAK-STAT pathways. We show that indigenous microbes mainly stimulate the Imd-Relish pathway, while pathogens trigger the activation of both the Imd-Relish and JAK-STAT pathways. Mutant analyses and functional genetics experiments revealed an essential role of conserved immune pathways in the control of ISC differentiation. Finally, by studying the relationship between these conserved immune pathways, we found that damage-mediated JAK-STAT activation antagonizes NF κ B's impact on ISC lineage. Overall, we propose that microbes affect ISC differentiation by altering the balance between PAMP-dependent innate immune activation (through Imd-Relish) and cytokine production induced by epithelial damage (through JAK-STAT). This mechanism plays a critical role in the determination of intestinal epithelial cellular structure.

RESULTS

The gut microbiota decreases the proportion of EEs in the midgut epithelium

A previous study suggested that indigenous microbes alter intestinal morphology and cell numbers (Broderick et al., 2014). To confirm this observation, we generated germ-free (GF) flies to determine the proportion of EEs among all differentiated cells (ratio EEs/(EEs + ECs)) in posterior midgut region 4. This EE ratio represents the fraction of differentiated cells that are EEs. We detected a 50% increase in the fraction of Prospero⁺ EEs in GF flies compared with their conventionally reared (CR) counterparts (Figures 1A and 1A'). This increase resulted in a matched increase in the total number of EEs (Figure 1A'') in GF compared with CR animals.

To determine if the microbiota-dependent change in epithelial composition is a consequence of altered ISC activity (and not a developmental effect), we generated Mosaic Analysis with a Repressible Cell Marker [Luo and Wu, 2007]) clones in GF and CR flies and quantified the fraction of EEs in the differentiated cells of the clones. The proportion of Prospero⁺ EEs was higher in GFP⁺ clone islets in the midgut of GF animals (Figures 1B, 1B', S1B, and S1B'), revealing that microbiota shifts ISC lineage toward EC fate. Smaller clone size (Figure 1C) might reflect diminished ISC proliferation in GF flies, which is consistent with our previous work (Buchon et al., 2009b).

Interestingly, the proportion of EEs in GF conditions reverted to the CR baseline in gnotobiotic flies re-associated with a minimal microbial community (Figure 1D) that included *Acetobacter tropicalis*, *Acetobacter pomorum*, *Lactobacillus plantarum*, *Lactobacillus brevis*, and *Lactobacillus fructivorans* (Chandler et al., 2011; Dobson et al., 2016). Next, we assessed if there was any single member of the microbiota specifically responsible for this effect. Re-association of *A. tropicalis* or *L. plantarum* in GF flies rescued the high proportion of EEs, but re-association of *L. brevis* or *E. faecalis* did not (Figure 1D). Both *A. tropicalis* and *L. plantarum* possess DAP-type PGN, while *E. faecalis* and *L. brevis* have Lys-type PGN (Lesperance and Broderick, 2020), suggesting that microbial PAMPs could be involved in this phenomenon. In conclusion, our results demonstrate that a subset of the gut microbiota influences gut epithelial cellular composition by affecting ISC lineage specification toward ECs.

Oral infection by pathogenic bacteria increases the proportion of EEs in the midgut epithelium

Indigenous microbes are not the only microbes affecting the intestinal epithelium. Oral infection with pathogens modulates cytokine signaling and epithelial turnover in the intestine (Buchon et al., 2009b). We next asked whether pathogens affect epithelium composition. Pathogens often induce a similar response to that of microbiota but one which is higher in magnitude. Ingestion of *Erwinia carotovora* ssp. *carotovora* 15 (*Ecc15*) generates damage to the midgut epithelium, which is compensated for by an acceleration of tissue renewal (Buchon et al., 2009b). In response to *Ecc15* ingestion, we detected an increase in both the number and proportion of Prospero⁺ EEs in the epithelium (Figures 2A, 2A', 2B, and S2A). We detected this increase of EE density in several wild-type *Drosophila melanogaster* strains with different magnitude (Figure S2B). In addition to changes in the posterior region of the midgut, region 4 (R4), which we measure throughout this article, we detected this increase of EEs also in anterior midgut region 2 (R2; Figure S2C). We asked whether this response could be an *Ecc15*-specific response or a common reaction to oral pathogens. To solve this question, flies were orally infected with *Pseudomonas entomophila* (*Pe*) or the human enteropathogen *Vibrio cholerae* (*Vch*), which are two other microbes that are pathogenic to *Drosophila* when ingested (Blow et al., 2005; Buchon et al., 2009b). We found a similar proportional increase in Prospero⁺ EEs after infection with both *Pe* and *Vch* (Figures 2A' and S2A), suggesting that alteration of epithelial cell composition is a conserved response to pathogenic insult.

It was recently shown that EEs represent a heterogeneous group of cells that could be classified based on the expression of distinct neuropeptides: class I EEs express Allatostatin C (AstC), while class II EEs produce Tachykinin (Tk) (Guo et al., 2019). Intriguingly, we found that a subset of EEs belonging to class I (but not class II) show robust accumulation during *Ecc15* infections (Figures S2D and S2D'), suggesting that the control of definite EE subclass accumulation is part of a pathogen-specific epithelial response. To explore whether EE accumulation is transient or long-lasting even after pathogens are eliminated from the gut, we sampled guts 2, 7, and 30 days post infection and quantified the proportion of EEs. Strikingly, we detected a significant increase in the proportion of EEs lasting for at least 30 days post infection (Figure 2C). Thus, our data demonstrate that ingestion of pathogens increases the proportion of EEs, suggesting that pathogenic and indigenous microbes have opposing effects.

A particularity of pathogens, compared with the microbiota, is that exposure to pathogens is associated with epithelial damage, cell loss, and increased ISC proliferation (Buchon et al., 2010). We hypothesized that “damage” could be required for the effect of pathogens on epithelial cell composition. To test this, we infected flies with an avirulent mutant *Ecc15* (*Ecc15^{evf-}*) (Quevillon-Cheruel et al., 2009), which did not promote an increase in the proportion of EEs (Figure 2D). This suggests that virulence-associated epithelial damage is required for EE accumulation. We next tested whether epithelial damage alone would be sufficient to stimulate an increase in the proportion of EEs. Ingestion of either dextran sodium sulfate (DSS) or bleomycin, two abiotic-damaging chemicals, led to a stable increase in the proportion of EEs in the epithelium (Figures 2E and S2E). Together, these results

demonstrate that epithelial damage is an essential component of pathogen-mediated changes in gut epithelial composition.

Ingestion of pathogens is associated with accelerated epithelium turnover, including massive loss and gain of cells, both of which could alter the proportion of EEs in the gut. To elucidate the contributions that cell gain and loss confer to our phenotype, we performed a time course experiment to monitor changes in cell composition. As early as 2 h post infection, we detected massive EC delamination into the lumen, whereas the EEs remained mostly basal (Figure S2F, yellow arrows and white asterisks, respectively). Simultaneously, we detected an increase in the proportion of EEs in the gut (Figure 2F). Around 8 h post infection, ISCs start to divide and differentiate to complete tissue regeneration by 48 h post infection (Buchon et al., 2010). We detected a second phase of increased EE proportions at the time of proliferation, and EEs remained constant for 4 days (Figure 2F). These results suggest that some of the change in the proportion of EEs is concomitant with ISC activity. Thus, we next tested whether ISCs alter their lineage upon infection. We generated twin-spot MARCM clones (Yu et al., 2009) in both unchallenged and *Ecc15*-infected guts and quantified Prospero⁺ EEs and ECs in each individual clone labeled by either GFP or RFP, respectively (Figure 2G). We found that the proportion of Prospero⁺ cells was higher in GFP- or RFP-labeled clones (Figure 2G') after *Ecc15* infection, revealing that pathogenic insult shifts ISC lineage toward EE fate. Thus, we propose that indigenous and pathogenic microbes oppositely influence ISC activity and alter ISC fate specification: the microbiota promotes EC fate, while pathogenic microbes promote EE fate, leading to an elevated density of these hormone-producing cells.

Microbes alter stem cell differentiation, leading to changes in epithelial cell composition

We next asked whether progenitor proliferation was either necessary or sufficient to change epithelial cell composition following pathogenic infection. We altered the rate of proliferation by modulating the epidermal growth factor receptor (EGFR) signaling pathway in *Escargot*⁺ (*Esg*⁺) progenitor cells, which is the main cell-autonomous regulator of ISC division upon infection (Buchon et al., 2010). Progenitor-specific depletion of EGFR via RNAi blocked both *Ecc15*-infection-induced proliferation and the increase in EEs (Figures 3A, 3B, and 3D-3E) and decreased the number of *Esg*⁺ cell numbers, probably via affecting EGFR-dependent EB survival (Reiff et al., 2019). This indicates that progenitor proliferation is necessary for EE accumulation upon pathogenic infection.

We also hyperactivated oncogenic Ras signaling by *Esg-Gal4*-driven overexpression of constitutively active Ras (Ras^{V12}), which induced ISC hyperproliferation in unchallenged animals ((Buchon et al., 2010), Figure 3D), and at similar proliferation rates as controls upon *Ecc15* infection (Figure 3D). ISC hyperproliferation alone did not induce changes in Prospero⁺ EE density in either unchallenged or *Ecc15*-infected animals (Figures 3C and 3E). These data reveal that proliferation of progenitors is required but not sufficient to alter epithelial composition.

Esg⁺ progenitors include two proliferative cell types, ISCs and EEP cells, the latter of which undergoes one mitotic division to produce a terminally differentiated pair of EEs (Chen et al., 2018). As *Ecc15* infection resulted in the formation of Prospero⁺ EE clusters

(Figure 3A), we next investigated the contribution of EEP mitosis toward infection-induced EE accumulation. We found that 10% of mitoses detected upon infection came from EEP mitosis (Figures S3A and S3B). *Pros*-specific depletion of EGFR reduced *Ecc15*-infection-induced EEP mitosis (Figures 3F and 3G) and produced only a minor effect on the total number of mitoses (Figure 3J). Blocking EEP mitosis had minimal impact on the *Ecc15*-induced increase in EEs (Figures 3H, 3I, and 3K), and Prospero⁺ EE clusters were still observed in these conditions (Figures 3H and 3I, insets). In addition, *Pros-Gal4*-driven hyperactivation of Ras signaling by the overexpression of constitutively active *Ras*^{V12} did not significantly alter gut proliferation or EE density in either unchallenged or *Ecc15*-infected animals (Figures S3C-S3E), suggesting that EEP mitosis is not a major driver of EE accumulation. In summary, our data indicate that ISC, but not EEP, proliferation is essential for the accumulation of EEs upon infection, but that EE proliferation alone is not sufficient to promote EE accumulation. This suggests that changes in ISC differentiation underlies pathogenic infection-induced gain of EEs.

The Imd-Relish pathway promotes EC fate by direct modulation of differentiation factors in progenitors

Most of the genes induced by microbiota are regulated by *Relish*, a conserved NFκB transcription factor downstream of the Imd-Relish pathway (Broderick et al., 2014). Recognition of bacteria by PGN-recognition protein LC (*PGRP-LC*) or *PGRP-LE* activates the pathway through intracellular signaling involving immune deficiency (*Imd*), which subsequently leads to Relish cleavage and nuclear translocation (Buchon et al., 2014). Cell-type-specific (Dutta et al., 2015) and single-cell (Hung et al., 2020) transcriptome datasets from *Drosophila* intestinal cells have shown that *Relish* is expressed in ISCs and EBs (Figures S4A and S4B). We confirmed that Relish protein is present in *Esg*⁺ progenitor cells and polyploid ECs (Figure S4C), in agreement with a previous study (Kamareddine et al., 2018). Since our results (Figure 1) suggested that members of the microbiota with DAP-type PGN, the PAMP that stimulates the Imd-Relish pathway, decrease the proportion of EEs in the epithelium, we thus hypothesized that the Imd-Relish pathway could impact ISC differentiation and thus epithelial composition. We found that the proportion of Prospero⁺ EEs was increased in *Relish*^{-/-} and *Imd*^{-/-} mutant flies compared with an isogenic control (Figures 4A, 4A', and S4D), but we detected no such change in *PGRP-LB*^{-/-} mutants (hyperactive Imd-Relish pathway [Charroux et al., 2018]). We further found that blocking Imd-Relish pathway activity in *Esg*⁺ progenitors by depletion of *Relish*, *PGRP-LE*, or *PGRP-LC* resulted in an increase in EE density (Figures 4B and 4B') without affecting ISC mitosis (Figure S4E) in young (7-day-old) flies. This finding was in line with a previous study showing no difference in mitotic activity of ISCs in 14- or 24-day-old flies after genetic modulation of the Imd-Relish pathway (Petkau et al., 2017). These results imply that the Imd-Relish pathway could regulate ISC differentiation cell autonomously and, consequently, gut epithelial composition.

In order to explore the transcriptional impact of *Relish* in progenitors, we employed two approaches aimed at identifying cell-specific direct targets (Figure 4C): (1) we isolated *Esg*⁺ cells by fluorescence-activated cell sorting (FACS) (Figure S4F) and analyzed the transcriptome of *Relish-IR* progenitors, and (2) we identified *Relish*-bound genes in

progenitors by targeted DamID (TaDa) (Marshall et al., 2016; Southall et al., 2013). These complementary approaches allowed us to identify genes regulated both directly and indirectly by Relish in progenitors, likely underlying its impact on ISC differentiation. We engineered transgenic flies expressing a Dam-Relish fusion under control of *UAS*. We verified that *Dam-Relish*, driven ubiquitously by *Daughterless-Gal4*, induces expression of the antimicrobial gene *Diptericin* when compared with *Dam-only* or *Dam-PolIII* controls (Figure S4G) and sequenced genes targeted by Rel-TaDa. In parallel, we performed RNA sequencing (RNA-seq) on FACS-sorted progenitors, either wild type (WT) or those knocked down for *Relish* by RNAi. Importantly, *Relish* was found significantly downregulated after *Esg*-specific *Relish-IR*, validating our transcriptomic dataset (Figure 4F). Altogether, we found 2,478 *Relish*-bound genes in intestinal progenitors of unchallenged flies and 187 downregulated genes in *Relish-IR* progenitors, from which 59 (31.5%) were both regulated and bound (including *Ret*; Figure 4E).

Gene Ontology (GO) categories related to cell differentiation, cell-fate specification, and stem cell and epithelial structure maintenance were enriched in both sets of genes regulated (Table S1) or were bound by *Relish* (Table S2; Figure 4D). From the 59 overlapping genes, *Gadd45*, *Stg*, and *Mthl14* were both bound and regulated, suggesting that *Relish* might be involved in the regulation of JNK stress signaling, cell-cycle control, and aging of ISCs. In addition, *Relish-IR* progenitor cells showed decreased expression of the *Notch* ligand *Delta*, the BMP-signaling receptor *Thickveins* (*tkv*), and the transcription factor *Sox21a* (Figure 4F), which were all bound by Relish (e.g., Figure S5A) and have all been shown to regulate ISC differentiation toward EC fate under physiological conditions (Chen et al., 2016; Ohlstein and Spradling, 2007; Tian et al., 2017; Tracy Cai et al., 2019). To validate our DamID and transcriptomic studies, we monitored the levels of Sox21a in progenitors using immuno-staining. Progenitor-cell-specific *Relish* knockdown decreased the level of Sox21a in *Esg*⁺ cells (Figure S5B). With a similar approach, we found that *relish* overexpression elevated, and *Relish* knockdown decreased, the level of Delta in *Esg*⁺ progenitor cells (Figures 4G and 4G'). Altogether, our results demonstrate that Relish in progenitors directly regulates the transcript and protein levels of key regulators of ISC differentiation.

The Notch pathway is a master regulator of EE/EC fate (Ohlstein and Spradling, 2007). We thus hypothesized that the Notch pathway could mediate some of the influence of Relish on epithelial composition. We analyzed the impact of ectopic Imd-Relish pathway activation on progenitor cells and analyzed the epistatic interactions between *Relish* and *Notch*. We found that activation of the Imd-Relish pathway by progenitor-cell-specific expression of *imd* decreases the proportion of EEs in unchallenged CR animals. Knockdown of *Notch* in progenitors leads to accumulation of tumor-like ISC/EB and Prospero⁺ EEs (Patel et al., 2015). Accordingly, we found that knockdown of *Notch* in progenitor cells strongly increased the proportion of EEs in the epithelium, and Imd-Relish pathway activation in the same progenitors did not rescue this phenotype (Figures 4H and 4H'). This is in line with previous data demonstrating that Imd-Relish pathway activation has no impact on grades of *Esg*-specific *Notch-IR*-initiated tumors (Petkau et al., 2017). These results suggest that the Imd-Relish pathway is sufficient to alter the proportion of EEs in the epithelium and that it acts upstream or in parallel to Notch signaling. Altogether, we conclude that Relish alters

ISC differentiation by transcriptionally stimulating classic regulators of ISC differentiation, including the Notch pathway.

The JAK-STAT pathway promotes EE-fate decisions in response to intestinal stress

Intriguingly, even though the Imd-Relish pathway promotes ISC differentiation toward EC fate, infection, which strongly stimulates the Imd-Relish pathway, is associated with the accumulation of EEs. It was previously shown that ingestion of *Ecc15* not only induces the Imd-Relish pathway, but damage due to infection also triggers the activation of the JAK-STAT pathway (Buchon et al., 2009a). JAK-STAT signaling plays a pivotal role in the humoral and cellular responses upon infection, as well as in stem cell homeostasis, cell fate, and tissue regeneration (Agaisse and Perrimon, 2004; Herrera and Bach, 2019). We therefore hypothesized that, upon infection, damage-associated induction of the JAK-STAT pathway could underly EE accumulation in the gut epithelium. Accordingly, we found that progenitor-specific overexpression of a constitutively active form of the JAK kinase Hopscotch (*Hop^{TumI}*) in unchallenged flies was sufficient to increase EE density (Figures 5A and 5B). Furthermore, *Esg-Gal4*-driven blockage of the JAK-STAT pathway by the overexpression of a dominant-negative form of the JAK-STAT receptor Domeless (*Domeless^{DN}*) decreased the proportion of EEs over ECs both in unchallenged conditions and upon infection with *Ecc15* (Figures 5A-5D). Our results indicate that JAK-STAT pathway activation is necessary and sufficient for the regulation of epithelial cellular composition during physiological conditions and upon infection.

It was previously reported that in conditions of stress, or in some mutant contexts, EEs could originate from Suppressor of hairless⁺ (*Su(H)⁺*) progenitors (EBs) instead of EEPs (Beehler-Evans and Micchelli, 2015; Hung et al., 2020; Korzelius et al., 2019). We thus aimed to determine whether the EEs that accumulated upon infection or upon JAK-STAT activation originated from EBs or EEPs. The T-TRACE system is a Gal4-regulated lineage-tracing system designed to identify stem cell progeny without the leakiness of the G-TRACE system (Figure S6) (Evans et al., 2009; Zeng and Hou, 2015). Using T-TRACE driven either in *Esg⁺* or *Su(H)⁺* progenitor cells, we detected new EEs formed only in the lineage of *Esg⁺* progenitors (Figures 5E, 5F, S7A, and S7B), but not of *Su(H)⁺* progenitors, demonstrating that, upon infection, EEs originated mostly from ISCs/EEPs and not EBs. ISCs oscillate between two states based on their expression of *Prospero* (*Esg⁺Pros⁻* or *Esg⁺Pros⁺*), and *Prospero* expression engages ISCs on the EE lineage. We next wanted to find in which of these ISC subpopulations JAK-STAT signaling is required in to give rise to excess EEs upon infection. *Pros^{TS}*-mediated overactivation of JAK-STAT signaling for 10 days did not result in excess EE formation (Figure S7C). Altogether, we propose that JAK-STAT activation in *Esg⁺Su(H)⁻Pros⁻* ISCs leads to the increase in the proportion of EEs observed upon infection.

The balance between Imd-Relish and JAK-STAT pathway activity determines ISC differentiation in response to microbes

Our data suggest that stimulation of the Imd-Relish pathway in ISCs promotes EC formation, while JAK-STAT activation stimulates EE formation. We therefore speculate that different microbial signals could uniquely influence epithelial composition. In such a

model, bacterial-derived PGN would stimulate EC fate while virulence-associated damage would trigger EE accumulation, and the balance of the Imd-Relish and JAK-STAT pathways mediates this effect. To explore this idea, we generated gut transcriptomes of GF and GF flies fed with high doses of either commensals (*A. tropicalis*, *L. plantarum*) or a pathogen (*Ecc15*). In GF animals, both pathways show relatively low activity as reported by the expression of their target genes and activating ligand (*AttacinD* [*attD*], *DiptericinB* [*DptB*] for Imd-Relish; *Suppressor of cytokine signaling at 36E* [*Socs36E*], *Unpaired3* [*Upd3*] for JAK-STAT) (Figures 6A and 6B). Feeding of different members of the microbiota community (*A. tropicalis*, *L. plantarum*) mostly activated the Imd-Relish, but not the JAK-STAT, pathway (Figures 6A and 6B; Table S4). In contrast, oral ingestion of pathogenic *Ecc15* activated both immune pathways (Figures 6A and 6B). In conclusion, while the indigenous microbiota activates the Imd-Relish pathway, pathogenic *Ecc15* triggers activation of both pathways.

Next, we aimed to elucidate the relationship among these two immune pathways during ISC differentiation. We monitored the proportion of EEs in GF, CR, and *Ecc15*-infected flies with either overactivated Imd-Relish or JAK-STAT pathways, specifically in *Esg*⁺ progenitor cells. *Esg*-specific *imd* overexpression was sufficient to reduce EE density in both GF and CR animals (Figure 6C), in agreement with its role in ISC differentiation toward ECs. Moreover, *Esg*-specific *relish* or *imd* overexpression suppressed the *Ecc15*-infection-induced increase in EE density, while *Relish* depletion (*Relish-IR*) had minimal impact (Figure 6D). These data suggest that the lack of activation of the Imd-Relish pathway activation in GF animals is responsible for the greater EE density, while upon infection, Imd activity is bypassed. In these conditions, an artificial increase in Imd activity can override JAK-STAT signaling activity. Furthermore, *Esg*-specific *imd* overexpression suppressed abiotic stress-mediated increase in EE density (Figure S8). Finally, JAK-STAT activation was sufficient (and necessary) to drive changes in epithelial cell composition, as *Esg*-specific *Hop*^{*Tuml*} expression led to increased EE density in unchallenged animals. Similarly, overexpression in infected animals resulted in even higher EE density than in WT animals (Figures 6E and 6F). Thus, we propose that the antagonistic effect of the JAK-STAT and Imd-Relish pathways determine ISC fate decisions and thus influence epithelial cellular composition in response to luminal microbes.

DISCUSSION

A central problem in gut biology is understanding the complex and reciprocal interactions between a host and its microbiome. An increasing number of studies suggest that intestinal microbes (microbiota or pathogens) are not only etiological factors for disease initiation and progression but are also key regulators of host physiology. Indeed, gut microbes have been shown to influence ISC activity and change intestinal morphology to reflect its environment (Buchon et al., 2009b; Peck et al., 2017). However, the mechanistic basis for microbial effects on ISC activity remains largely unexplored. In this study, we found that indigenous and pathogenic microbes oppositely influence ISC differentiation and epithelial cellular composition through differential modulation of classical immune pathways. This molecular dialogue determines ISC behavior via the balanced activity of pathways involved in microbial pattern (PAMPs) recognition (i.e., Imd-Relish) and epithelial damage (damage-

associated molecular patterns [DAMPs]) detection (i.e., JAK-STAT), which, together, consequently influence ISC differentiation, epithelial composition, and gut physiology. Our study identifies a crosstalk between immune and developmental pathways in stem cells as the center of the communication network between a host and its gut microbes.

Microbiota and pathogens oppositely shape gut epithelial structure by altering ISC differentiation

Morphological and structural changes of the intestine have been described in GF mice and flies accompanied by a lower rate of ISC mitosis, reduced tissue turnover, and altered EE numbers (Broderick et al., 2014; Round and Mazmanian, 2009). In this study, we demonstrate that microbes control the intrinsic differentiation program of ISCs, thereby influencing the proportion of terminally differentiated cell types and epithelial structure. In mammals, a recent single-cell survey of mouse small intestinal epithelium revealed that pathogenic *Salmonella enterica* infection provokes an increase in the proportion of secretory Paneth cells (Haber et al., 2017). Moreover, infection by parasitic helminth (*Nippostrongylus brasiliensis*) promotes elevated proportions of secretory goblet and tuft cells in the small intestine and alters epithelial cell architecture via the action of secreted interleukin-25 on crypt progenitors (Miller and Nawa, 1979; Von Moltke et al., 2016). These data suggest that the impact of microbes and an infection by pathogens on epithelial cell composition is conserved. Intriguingly, our results show that the microbiota suppresses EE fate while pathogenic microbes stimulate it. It remains unclear whether this divide is adaptive for either the host or the pathogens. However, it has been previously shown that EEs contribute to the elimination of microbes from the midgut (Ye et al., 2021). It is therefore possible that EE accumulation upon infection allows the host to make the gut environment more hostile to microbes, either through immune or physiological changes, as part of the response to pathogens. Conversely, a decrease in EEs could promote tolerance to non-pathogenic microbes by generating a less hostile luminal milieu. Importantly, in natural conditions, the gut ecosystem harbors numerous microbes that coexist and include bacteria with different levels of virulence/pathogenicity. The opposite influence of these two pathways could indicate that the ratio of microbes and microbial damage is constantly monitored in the gut and influences epithelial composition. Such a model would explain how dysbiosis or chronic inflammation in the gut could lead to not only altered gut homeostasis but aberrant gut structure as well (Olafsson et al., 2020).

Activated by microbes, the *Drosophila* NF κ B transcription factor Relish directly regulates ISC differentiation toward the EC fate. Oppositely, pathogenic-infection-triggered damage led to cytokine-mediated JAK-STAT activation upon tissue repair, which overrides NF κ B's effect on epithelium structure. These data confirm that the JAK-STAT pathway is a major regulator of ISC differentiation in the gut (Beebe et al., 2010). Importantly, the JAK-STAT pathway is required for ISC differentiation in general, and a lack of JAK-STAT has been associated with differentiation defects (Jiang et al., 2009). Key regulators of EC fate are proposed to be regulated by the JAK-STAT pathway in progenitor cells (Jiang et al., 2009), but we found that activation of JAK-STAT in progenitors leads to an increase in EE production. This suggests that the JAK-STAT pathway could have multiple roles in progenitors, first required for general differentiation but also important for the specification

of EEs. We also found that another key immune pathway, the Imd-Relish pathway, regulates ISC differentiation in an opposite manner. These findings suggest that immune pathways could have a general role in the regulation of ISCs. Strikingly, NF κ B and STAT3 are key regulators of mammalian gut homeostasis: both are inflammatory bowel disease (IBD)-associated genes and contribute to abnormal digestive-system morphology and celiac disease in humans (Jostins et al., 2012; McGovern et al., 2010). Moreover, NF κ B activation proved to be critical for progenitor hyperproliferation and transformation upon colorectal cancer initiation following *Adenomatous Polyposis Coli* (*APC*) mutation (Myant et al., 2013). Thus, we believe that our findings establish a molecular linchpin between a conserved regulatory mechanism responding to pathogenic infection and subsequent tissue repair, which could potentially be exploited to understand the complex etiology of diseases that drive tumorigenesis.

Intestinal EEs: Regulators of host defense and physiology?

Drosophila intestinal EEs secrete a wide spectrum of neuropeptides modulating intestinal physiology and growth and are central to the interaction between diet and hormonal regulation (Amcheslavsky et al., 2014; Guo et al., 2019). An EE-specific Imd-Relish pathway has been found to control the expression of the endocrine peptide Tk in response to microbe-derived acetate, which ultimately regulates lipid metabolism, insulin signaling, and host development (Kamareddine et al., 2018). Therefore, it is plausible that, beyond sensing nutrients, EEs are also continuously sampling microbe-derived molecules and orchestrate host responses including epithelial immunity, metabolism, and gut physiology. Accordingly, recent studies have demonstrated that mouse and zebrafish intestinal EEs sense pro-inflammatory bacterial compounds and tryptophan catabolites and consequently activate hormone secretion, which promotes intestinal motility and pathogen clearance (Lebrun et al., 2017; Ye et al., 2021). Further studies are required to determine the molecular mechanisms regulating EE activity, response specificity, and communication circuits.

The long-lasting robust doubling of EEs described in this study as a response to pathogenic infection demonstrates that damage and infection could have long-term consequences for host physiology. One could speculate that such a phenomenon might have two important consequences. First, it could provide some form of “immunological memory” preserved at the level of altered intestinal epithelium structure. In such a model, cellular composition, in addition to immune induction, would influence how the host can deal with future challenges, especially infection. This would imply that reshaping epithelial structure is an integral part of the immune response, rather than an indirect consequence of cellular damage. In that context, accumulating certain epithelial cell populations upon infection would be a response analogous to the accumulation of immune cells at the site of infection/inflammation. A second consequence would be that damage and infection could durably alter the intimate relationship between the microbiota and its host. In such a model, a primary insult would trigger structural changes to the gut, which could alter the risk of dysbiosis. Conversely, dysbiosis could further promote inflammation and alter the gut environment, generating a vicious cycle leading to inflammatory disorders. Such crosstalk between microbiota and gut homeostasis would be particularly relevant during age-related deterioration of the intestinal epithelium, when aberrant ISC differentiation and dysbiosis impair tissue function (Biteau

et al., 2008; Buchon et al., 2009b; Choi et al., 2008; Liu et al., 2017). We propose that this immune-developmental crosstalk could contribute to age-related dysplasia. It has been shown during aging that the capacity to combat infection decreases and therefore microbial load increases (Müller et al., 2013). Microbe-dependent Imd-Relish and JAK-STAT pathway activation during aging has also been previously reported in the midgut as contributing to gut-structure disorganization (Buchon et al., 2009b). We therefore propose that progressive dysbiosis could lead to a shift in the balance between Imd-Relish and JAK-STAT pathways and to an imbalance in EE versus EC differentiation during aging. Altogether, our work demonstrates that the influence of gut microbes on their host is not exclusively mediated by a direct, reversible impact on gut physiology. Rather, gut microbes can influence and re-program stem cells by modulating immune signaling, leading perhaps to long-lasting alterations of gut structure and function.

Limitations of the study

Similar to previous papers studying cell-type-specific transcription factor target sites, we identified more putative Relish target genes by DamID than downregulated genes after Relish-IR by an RNA-seq approach. This could happen because regulation of gene expression may not directly follow binding. Another possibility is that the target gene expression is very low in the cell of interest and RNA-seq approaches are not sensitive enough to capture differences in expression. In addition, our work on the molecular mechanisms of EE accumulation is limited to one region of the midgut. Future work should address how gut regionalization affects this phenotype.

STAR★METHODS

RESOURCE AVAILABILITY

Lead contact—All the materials used in this study are publicly available. Further information and requests for resources and reagents should be directed to and will be fulfilled by the lead contact, Nicolas Buchon (nicolas.buchon@cornell.edu).

Materials availability—All unique/stable reagents generated in this study are available from the lead contact without restriction.

Data and code availability

- RNAseq and DamID data have been deposited at SRA and are publicly available as of the date of publication. Accession numbers are listed in the key resources table. Microscopy data reported in this paper will be shared by the lead contact upon request.
- This paper does not report original code.
- Any additional information required to reanalyze the data reported in this paper is available from the lead contact upon request.

EXPERIMENTAL MODEL AND SUBJECT DETAILS

Fly stocks and husbandry—All fly stocks were maintained at room temperature (~23°C) on standard (Cornell diet) corn meal and yeast extract medium (sucrose, cornmeal, yeast, and agar), with light-cycle control. Fly lines: Wild-type controls: *Canton S*, *w¹¹¹⁸*, *Hikone-A-W* (BDSC4), *Oregon-R-P2* (BDSC2376), *DGRP-391* (BDSC25191), *DGRP-859* (BDSC25210). Mutant lines: *Rel^{E20}*; *ImdR¹⁵⁶* (Hedengren et al., 1999); *PGRP-LE¹¹²*/*LC^{E12}* (Takehana et al., 2004); *PGRP-LB KO* (Paredes et al., 2011), backcrossed to *Canton S* background. Gal4 Drivers: *tub-Gal80^{TS}*; *Da-Gal4* (ubiquitous, BDSC86326); *Esg-Gal4/CyOlacZ*; *UAS-GFP, tub-Gal80^{TS} (Esg^{TS}*, ISC and EB-specific); *Su(H)GBE-Gal4*; *UAS-GFP, tub-Gal80^{TS} (Su(H)^{TS}*, EB-specific) (Jiang et al., 2009); *UAS-GFP, tub-Gal80^{TS}; prosv1-Gal4/TM6B (Pros^{TS}*, EE and EEP-specific) (Zeng et al., 2010); UAS-transgenic lines: *UAS-Imd*; *UAS-Rel* (Georgel et al., 2001); *UAS-RasV12* (BDSC4847); *UAS-Dome-DN*; *UAS-Hop^{Tum1}* (Harrison et al., 1995); *UAS-nls-GFP* (BDSC4775); *TI{2A-GAL4}AstC[2A-GAL4]* (BDSC84595); *TI{2A-GAL4}Tk[2A-GAL4]* (BDSC84693); UAS-RNAi lines: *UAS-Rel-IR* (BDSC33661, BDSC28943); *UAS-PGRP-LE-IR* (BDSC60038); *UAS-PGRP-LC-IR* (BDSC33383); *UAS-Notch-IR* (BDSC33611); *UAS-EGFR-IR* (BDSC25781). Conditional Gal4^{TS}-induced overexpression and knock-down flies were obtained by crossing virgin females of the strain containing the driver/TS system with males containing the UAS-transgene line. F1 progenies (driver > UAS-transgene) were raised at 18°C until 3 days after emergence, to allow for gut development. Flies were then transferred to 29°C for at least 7 days to allow for maximum transgene expression and RNAi-mediated gene knockdown.

Dam-Relish cloning, generation of Dam-Relish flies—The full sequence of Relish was amplified by PCR using BDGP Gold cDNA clones-GH01881 as template (Drosophila Genomics Resource Center). The following primer sequences were used for PCR: forward primer: GCGGCCGCGGATGAACATGAATCAGTACTACG; reverse primer: CGGCCGAGTCAAGTTGGGTTAACCAGTAG. Then, the full sequence of Relish was cloned into plasmid pUAST-attB-LT3-NDam (Marshall et al., 2016), which is a gift from Dr. Andrea Brand. PUAST-attB-LT3-NDam-Relish was integrated on the third chromosome by BestGene Inc.

METHOD DETAILS

Lineage tracing

T-TRACE: This lineage-tracing system is controlled by both temperature shift and estrogen induction (Zeng and Hou, 2015). The following lines were used to perform lineage-tracing experiments: *Tub-Gal80^{TS}, UAS-cre-EBD³⁰⁴* (carrying thermo-sensitive Gal80 and estrogen inducible Cre recombinase); *Esg-Gal4, Ubi-p63e-loxP-stop-loxP-GFP* (for tracing progeny of ISCs and EBs); *Su(H)GBE-Gal4, Ubi-p63e-loxP-stop-loxP-GFP* (for tracing progeny of EBs) (Zeng and Hou, 2015). Crosses and F1 progeny were cultured on regular food without estrogen at 18°C. 3–5 days old F1 flies were shifted to 29°C and transferred to food containing 150µg/mL estrogen for 7 days to initiate the lineage-tracing experiment. Oral infection for 3 days was carried out as described below before dissection.

G-TRACE: This lineage-tracing system was used to label the progeny of EBs. EB-specific Gal4-driver (*Su(H)^{TS}*) was crossed to *UAS-RedStinger*, *UAS-FLP*, *Ubi-p63(FRT.STOP)Stinger* (BDSC28280) at 18°C. 3–5 days old F1 flies were shifted to 29°C for 7 days to initiate lineage tracing. Oral infection for 3 days was carried out as described below before dissection.

Bacterial cultures and oral infection—*Erwinia carotovora ssp. carotovora 15 (Ecc15)* and *Pseudomonas entomophila (Pe)* are two Gram-negative bacteria, pathogenic to the *Drosophila* midgut when ingested (Buchon et al., 2013a). Human enteropathogen *Vibrio cholerae (VCh; serotype O1 biotype EIT or strain N16961)* causes cholera disease by producing an enterotoxin (Faruque et al., 1998). *Ecc15* and *VCh* were maintained on standard LB agar plates, and *Pe* was maintained on LB agar plates with 10% skimmed milk. *Pe* was plated from glycerol stocks for each experiment. Bacteria were inoculated in LB medium at 29°C for 16 hours and pelleted to OD₆₀₀ = 200. Oral infection was performed following previously described protocol (Buchon et al., 2009b): conventionally reared flies were starved in empty vials for 2 hours at 29°C, then moved to infection vials in which the fly food was covered by a Whatman filter paper containing 150µL of either 2.5% sucrose solution (control), or mixed solution of 75µL 5% sucrose with equal volume OD₆₀₀ = 200 bacterial pellet, or a solution of 500µg/mL of bleomycin or 6% DSS. For bacterial mono-association experiments (Figure 1D) GF flies were starved for 2 hours at 29°C, then moved to vials in which the fly food was covered by a Whatman filter paper containing 150µL of either 2.5% sterile sucrose solution (GF), or a mixed solution of 75µL 5% sterile sucrose with equal volume OD₆₀₀ = 200 bacterial pellet (*Acetobacter tropicalis - Atro*, *Lactobacillus plantarum - Lpla*, *Enterococcus faecalis - Ef*). All treated flies were incubated at 29°C until dissection. For transcriptome analysis: germ free flies were starved for 2 hours at 29°C, then moved to vials in which the fly food was covered by a Whatman filter paper containing 150µL of either a 2.5% sucrose solution (control), or a mixed solution of 75µL 5% sucrose with equal volume OD₆₀₀ = 200 bacterial pellet (*Acetobacter tropicalis - Atro*, *Lactobacillus plantarum - Lpla*, *Erwinia carotovora ssp. carotovora 15 - Ecc15*). GF flies were transferred to OD₆₀₀ = 100 bacterial pellet-containing vials for 5 days before dissection and immunostaining to assess effect of microbiota. Conventionally-reared flies were used to identify differences in gene expression between CR and GF conditions.

MARCM, twin-spot MARCM clone induction—Fly lines used: *hsMARCMFRT82B (hsFlp, tub-Gal4-UAS-GFP; FRT82B, tub-Gal80); BDSC5619:y[d2] w[1118]; P{ry[+t7.2] = ey-FLP.N}2 P{GMR-lacZ.C(38.1)}TPN1; P{ry[+t7.2] = neoFRT}82B*; twin-spot MARCM: *yw; FRT40A UAS CD8 RFT, UAS CD2-Mir/CyO; tubGal4, tubgal80ts/TM6C and hsfIp; FRT40A UAS CD2 RFT, UAS GFP-Mir/CyO*. For the MARCM assay, the F1 progeny from the crossing of the two lines was used for clone induction. 3–5-day-old flies with the appropriate genotypes were heat-shocked for 1 hour at 37°C in a water bath. The flies were then immediately transferred into a new tube and kept at room-temperature for 10 days before dissection. For the Twin spot infection assay, the F1 progeny from the crossing of the two lines was used for clone induction. Developing flies were kept at 18°C. Upon eclosion, flies were transferred to a new vial, and kept at 18°C for four days to allow for gut maturation. On the fourth day, flies were treated for infection as described below. During

the starvation included in the infection procedure, flies were heat shocked at 37°C in a water bath for 30 min. Infected flies were then dissected at 48 hours post infection, and unchallenged flies were dissected 1 week post mock procedure, to account for slower clone growth.

Generation of germ-free flies—Fresh fruit juice agar plates were made from grape agar powder premix packets (Flystuff, 47-102). Adult flies were transferred on fresh fruit juice agar plates supplemented with yeast paste. After 1 day of habituation, flies were allowed to lay eggs for 4 hours on agar plates. Eggs were collected gently with brush and were first suspended in 1X PBS, rinsed in 70% EtOH for 1 minute and dechorionated using 10% bleach for ~10min. Eggs were then transferred under a UV sterilized flow hood and further rinsed 3 times with sterile ddH₂O. The eggs were finally collected into sterile fly vials with sterilized food. Adult flies were tested for presence of bacteria after each experiment, by plating homogenates on MRS agar plates.

Immunohistochemistry and fluorescence imaging—Dissected *Drosophila* midguts were fixed in 4% paraformaldehyde in 1X PBS for 40 minutes and subsequently washed 3 times with 0.1% TritonX in PBS. The samples were then incubated for 3 hours in blocking solution (3% bovine serum albumin in 1X PBST). The midguts were then incubated with primary antibody at 4°C overnight. Samples were washed with 0.1% TritonX in PBS and incubated 2 hours with secondary antibodies. Primary antibodies used: chicken anti-GFP (1:1500, Thermo Fisher, A10262), mouse anti-Prospero (1:100, DSHB, MR1A), mouse anti-Delta (1:100, DSHB, C594.9B), rabbit anti-Relish (1:1000, Ray-Biotech, ABIN1111036), Alexa Fluor 555 Phalloidin (1:2000, Thermo Fisher, R415), rabbit anti-Sox21a (1:300) (Meng and Biteau, 2015) and rabbit anti-PH3 (1:1000, EMD Millipore, 06-570). Secondary antibodies used: donkey anti-mouse-555 (1:2000, Thermo Fisher, A31570), donkey anti-rabbit-555 (1:2000, Thermo Fisher, A21206), donkey anti-mouse-647 (1:1000, Thermo Fisher, A31571), donkey anti-rabbit-647 (1:1000, Thermo Fisher, A31572) and goat anti-chicken-488 (1:2000, Thermo Fisher, A11039). Nuclear DNA was stained in 1:50,000 DAPI (Sigma-Aldrich, D9564) in PBS for 30min, and samples were finally washed three times in PBS before mounting in antifade medium (Citifluor AF1, EMS, 17970-100). All imaging was performed on a Zeiss LSM 700 fluorescent/confocal inverted microscope. Semi-automated cell counts were performed with Fiji (Schindelin et al., 2012).

Escargot-GFP⁺ cell sorting—*Escargot-Gal4; tub-Gal80^{TS}* (ISC- and EB-specific driver) was crossed with wild type control CantonS or Relish-RNAi line at 18°C. F1 progenies were kept at 18°C for three days before shifting to 29°C. Seven days later, about 200 midguts from female flies were dissected. Elastase (Sigma-Aldrich E0258-10mg) was used to disassociate cells from tissue, and GFP⁺ ISC and EB cells were then collected using BD FACSAria Fusion flow cytometry instrument (Cornell Biotechnology Resource Center). All processes were performed following published protocol (Dutta et al., 2015). Total RNA was extracted from collected cells, followed by cDNA library preparation and Illumina HiSeq2500 sequencing (Cornell Biotechnology Resource Center).

RNA-seq analysis—Oral infection of GF adult flies was performed as described above. 50 guts per condition were dissected 6 hours post-treatment and immediately transferred into Trizol (Life Technologies 15596018) kept on ice and subsequently homogenized and stored at -80°C . Total RNA was isolated from midguts or sorted cells following using a hybrid Trizol-RNeasy (Qiagen RNeasy Mini kit Cat No./ID: 74106) protocol. RNA-Seq libraries were built using the Quantseq 3' mRNA-Seq kit (Lexogen) and sequencing was performed on an Illumina HiSeq instrument maintained at Cornell Institute of Biotechnology Genomics Core Facility. As we have previously published, reads were mapped to the host genome using STAR and differences in expression levels among treatments have been inferred using CuffDiff and DESeq2 (Houtz et al., 2017, 2019; Troha et al., 2018). Raw high throughput sequencing data are deposited to SRA repository under accession numbers: SRA: PRJNA757772 and SRA: PRJNA779708.

RT-qPCR—Total RNA was extracted from 20 female fly midguts using the standard TRIzol (Invitrogen) extraction. RNA samples were treated with PERFECTA DNaseI (Quanta #95150-01K), and cDNA was generated using qScript cDNA Synthesis Kit (Quantabio #95047-100). qPCR was performed using PerfeCTa SYBR Green FastMix (Quanta Biosciences # 95072-012) in a Bio-Rad CFX-Connect instrument. Data represent fold change between the relative ratio of the target gene and that of the reference gene RpL32. Mean values of at least three biological replicates are represented \pm SE. The oligonucleotide sequences used can be found in our previous publication (Troha et al., 2019).

Targeted DamID in Escargot⁺ cells—*Escargot-Gal4; tub-Gal80^{TS}* (ISC- and EB-specific driver) flies were crossed to UAST-LT3-NDam and UAST-LT3-NDam-Relish flies at 18°C . 3-5 days old progeny were collected and aged for a further 3 days at 18°C before shifting to 29°C to induce Dam and Dam-Relish protein expression for 48 hours. 50 midguts per repeat were dissected in ice-cold PBS and stored at -80°C . Methylated fragments were isolated and sequencing libraries were prepared as published before (Marshall et al., 2016; Southall et al., 2013) and briefly described below.

DamID library preparation, sequencing and data analysis—Genomic DNA was isolated using DNeasy Blood and Tissue kit (Qiagen Cat No./ID: 69506) and digested overnight with DpnI (New England Biolabs R0176S). DamID adaptors (see Table S1) were then ligated to DpnI digested DNA using T4 DNA ligase (New England Biolabs M0202S) and subsequently digested with DpnII (New England Biolabs R0543S). Ligated fragments were enriched by PCR amplification using Advantage2 polymerase (Clontech 639201). Sample shearing to $\sim 300\text{bp}$ fragment size was carried out at Cornell Institute of Biotechnology Core Facilities using Covaris E220 sonicator (Covaris microtube 520045). DamID adaptors were removed by AlwI (New England Biolabs R0513S) overnight digestion. AMPure XP magnetic beads (Beckman Coulter A63880) were used for cleanup for sequencing library preparation. After adjusting sample concentrations, end repair and 3' end adenylation, sequencing adaptors (see Table S3) were ligated using NEB quick ligase enzyme (New England Biolabs M2200S). After two rounds of DNA cleanup for sequencing library preparation DNA fragments were enriched by PCR amplification using NGS primers

(see Table S3) and NEBNext High Fidelity PCR Mix (New England Biolabs M0541S). After cleanup, quality control and library pooling were carried out at Cornell Institute of Biotechnology Genomics Core Facility. 75bp single-end reads were obtained via Illumina NextSeq500 instrument. Libraries were multiplexed to yield at least 20 million mapped reads per sample. Analysis of DamID data was performed as published recently (Marshall and Brand, 2015; Marshall et al., 2016). Gene Ontology over-representation analysis was performed using the online tool Panther. Raw high throughput sequencing data are deposited to SRA repository under accession number: SRA: PRJNA736303.

QUANTIFICATION AND STATISTICAL ANALYSIS

Data analysis, graph generation and figure assembly were performed in R and Adobe Photoshop (23.1.1 Adobe). Confocal images were analyzed using ImageJ (Version: 2.0.0-rc-69/1.52p) to quantify EE and EC cell numbers in gut Region 4 (Buchon et al., 2013b). Mitotic cells (PH3-positive cells labelled with a far-red probe) were manually counted. Relish binding peaks were visualized in IGV (Integrative Genomics Viewer V2.5.3). 1-2 μ m Z-stack slices from each image have been analyzed in ImageJ and number of ECs were determined based on nuclei size. This allowed us to capture all cells even upon multilayering which happen during progenitor-specific overexpression of *Ras*^{V12} when newly differentiated cells are produced at higher rate than normally (Jiang et al., 2011). Three biological replicates were performed. Violin plots include 0.25, 0.5, 0.75 quantiles and mean represented by black lines and yellow diamond, respectively. Results were analyzed using a two-way ANOVA followed with Tukey's posthoc-tests or Kruskal-Wallis followed Wilcoxon rank sum exact test with Benjamini-Hochberg posthoc-tests for specific comparisons or Student's t test (*p < 0.05, **p < 0.01, ***p < 0.001, ****p < 0.0001). For Figures 3E, 3K, S2B, S2C, S3E and S8 we used generalized linear mixed models to compare difference between infection or genotype. We tested the difference between main effect by comparing log-likelihood of the complete model to a model lacking the main effect to calculate p-values (****p < 0.0001, ns: non-significant).

Supplementary Material

Refer to Web version on PubMed Central for supplementary material.

ACKNOWLEDGMENTS

We would like to thank the following people for sharing resources: Tobi Doerr (*Vch* strain N16961), Benoit Biteau (Sox21a antibody), and Andrea Brand (TaDa flies and plasmid). We thank members of the N.B. lab for helpful comments on the manuscript. This work was supported by NSF IOS-1656118, NSF IOS-2024252, NIH 5R21AG065733-02, and NIH 1R01AI148541-02 to N.B.

REFERENCES

- Agaisse H, and Perrimon N (2004). The roles of JAK/STAT signaling in *Drosophila* immune responses. *Immunol. Rev* 198, 72–82. [PubMed: 15199955]
- Akira S, Uematsu S, and Takeuchi O (2006). Pathogen recognition and innate immunity. *Cell* 124, 783–801. [PubMed: 16497588]

- Amcheslavsky A, Song W, Li Q, Nie Y, Bragatto I, Ferrandon D, Perrimon N, and Ip YT (2014). Enteroendocrine cells support intestinal stem-cell-mediated homeostasis in *Drosophila*. *Cell Rep.* 9, 32–39. [PubMed: 25263551]
- Apidianakis Y, and Rahme LG (2011). *Drosophila melanogaster* as a model for human intestinal infection and pathology. *Dis. Model. Mech* 4, 21–30. [PubMed: 21183483]
- Beebe K, Lee WC, and Micchelli CA (2010). JAK/STAT signaling coordinates stem cell proliferation and multilineage differentiation in the *Drosophila* intestinal stem cell lineage. *Dev. Biol* 338, 28–37. [PubMed: 19896937]
- Beehler-Evans R, and Micchelli CA (2015). Generation of enteroendocrine cell diversity in midgut stem cell lineages. *Development* 142, 654–664. [PubMed: 25670792]
- Bernstein CN, Blanchard JF, Kliewer E, and Wajda A (2001). Cancer risk in patients with inflammatory bowel disease: a population-based study. *Cancer* 91, 854–862. [PubMed: 11241255]
- Biteau B, and Jasper H (2014). Slit/Robo signaling regulates cell fate decisions in the intestinal stem cell lineage of *Drosophila*. *Cell Rep.* 7, 1867–1875. [PubMed: 24931602]
- Biteau B, Hochmuth CE, and Jasper H (2008). JNK activity in somatic stem cells causes loss of tissue homeostasis in the aging *Drosophila* gut. *Cell Stem Cell* 3, 442–55. [PubMed: 18940735]
- Blow NS, Salomon RN, Garrity K, Reveillaud I, Kopin A, Jackson FR, and Watnick PI (2005). *Vibrio cholerae* infection of *Drosophila melanogaster* mimics the human disease cholera. *PLoS Pathog.* 1, e8. [PubMed: 16201020]
- Broderick NA, Buchon N, and Lemaitre B (2014). Microbiota-induced changes in *drosophila melanogaster* host gene expression and gut morphology. *MBio* 5, e01117–14.
- Buchon N, Broderick NA, Poidevin M, Pradervand S, and Lemaitre B (2009a). *Drosophila* intestinal response to bacterial infection: activation of host defense and stem cell proliferation. *Cell Host Microbe* 5, 200–211. [PubMed: 19218090]
- Buchon N, Broderick NA, Chakrabarti S, and Lemaitre B (2009b). Invasive and indigenous microbiota impact intestinal stem cell activity through multiple pathways in *Drosophila*. *Genes Dev.* 23, 2333–2344. [PubMed: 19797770]
- Buchon N, Broderick NA, Kuraishi T, and Lemaitre B (2010). *Drosophila* EGFR pathway coordinates stem cell proliferation and gut remodeling following infection. *BMC Biol.* 8, 152. [PubMed: 21176204]
- Buchon N, Broderick NA, and Lemaitre B (2013a). Gut homeostasis in a microbial world: insights from *Drosophila melanogaster*. *Nat. Rev. Microbiol* 11, 615–626. [PubMed: 23893105]
- Buchon N, Osman D, David FPA, Yu Fang H, Boquete JP, Deplancke B, and Lemaitre B (2013b). Morphological and molecular characterization of adult midgut compartmentalization in *Drosophila*. *Cell Rep.* 3, 1725–1738. [PubMed: 23643535]
- Buchon N, Silverman N, and Cherry S (2014). Immunity in *Drosophila melanogaster*—from microbial recognition to whole-organism physiology. *Nat. Rev. Immunol* 14, 796–810. [PubMed: 25421701]
- Chandler JA, Lang J, Bhatnagar S, Eisen JA, and Kopp A (2011). Bacterial communities of diverse *Drosophila* species: ecological context of a host-microbe model system. *PLoS Genet.* 7, e1002272. [PubMed: 21966276]
- Charroux B, Capo F, Kurz CL, Peslier S, Chaduli D, Viallat-lieutaud A, and Royet J (2018). Cytosolic and secreted peptidoglycan-degrading enzymes in *Drosophila* respectively control local and systemic immune responses to microbiota. *Cell Host Microbe* 23, 215–228.e4. [PubMed: 29398649]
- Chen J, Xu N, Huang H, Cai T, and Xi R (2016). A feedback amplification loop between stem cells and their progeny promotes tissue regeneration and tumorigenesis. *Elife* 5, e14330. [PubMed: 27187149]
- Chen J, Xu N, Wang C, Huang P, Huang H, Jin Z, Yu Z, Cai T, Jiao R, and Xi R (2018). Transient Scute activation via a self-stimulatory loop directs enteroendocrine cell pair specification from self-renewing intestinal stem cells. *Nat. Cell Biol* 20, 152–161. [PubMed: 29335529]
- Choi N-H, Kim J-G, Yang D-J, Kim Y-S, and Yoo M-A (2008). Age-related changes in *Drosophila* midgut are associated with PVF2, a PDGF/VEGF-like growth factor. *Aging Cell* 7, 318–334. [PubMed: 18284659]

- Dobson AJ, Chaston JM, and Douglas AE (2016). The *Drosophila* transcriptional network is structured by microbiota. *BMC Genomics* 17, 975. [PubMed: 27887564]
- Dutta D, Dobson AJ, Houtz PL, Gläßer C, Revah J, Korzelius J, Patel PH, Edgar BA, and Buchon N (2015). Regional cell-specific transcriptome mapping reveals regulatory complexity in the adult *Drosophila* midgut. *Cell Rep.* 12, 346–358. [PubMed: 26146076]
- Dyson JK, and Rutter MD (2012). Colorectal cancer in inflammatory bowel disease: what is the real magnitude of the risk? *World J. Gastroenterol* 18, 3839–3848. [PubMed: 22876036]
- Evans CJ, Olson JM, Ngo KT, Kim E, Lee NE, Kuoy E, Patananan AN, Sitz D, Tran PT, Do MT, et al. (2009). G-TRACE: rapid Gal4-based cell lineage analysis in *Drosophila*. *Nat. Methods* 6, 603–605. [PubMed: 19633663]
- Faruque SM, Albert MJ, and Mekalanos JJ (1998). Epidemiology, genetics, and ecology of toxigenic *Vibrio cholerae*. *Microbiol. Mol. Biol. Rev* 62, 1301–1314. [PubMed: 9841673]
- Georgel P, Naitza S, Kappler C, Ferrandon D, Zachary D, Swimmer C, Kopczynski C, Duyk G, Reichhart JM, and Hoffmann JA (2001). *Drosophila* immune deficiency (IMD) is a death domain protein that activates antibacterial defense and can promote apoptosis. *Dev. Cell* 1, 503–514. [PubMed: 11703941]
- Guo X, Yin C, Yang F, Zhang Y, Huang H, Wang J, Deng B, Cai T, Rao Y, and Xi R (2019). The cellular diversity and transcription factor code of *Drosophila* enteroendocrine cells. *Cell Rep.* 29, 4172–4185.e5. [PubMed: 31851941]
- Haber AL, Biton M, Rogel N, Herbst RH, Shekhar K, Smillie C, Burgin G, Delorey TM, Howitt MR, Katz Y, et al. (2017). A single-cell survey of the small intestinal epithelium. *Nature* 551, 333–339. [PubMed: 29144463]
- Harrison DA, Binari R, Nahreini TS, Gilman M, and Perrimon N (1995). Activation of a *Drosophila* Janus kinase (JAK) causes hematopoietic neoplasia and developmental defects. *EMBO J.* 14, 2857–2865. [PubMed: 7796812]
- Hedengren M, Åsling B, Dushay MS, Ando I, Ekengren S, Wihlborg M, and Hultmark D (1999). Relish, a central factor in the control of humoral but not cellular immunity in *Drosophila*. *Mol. Cell* 4, 827–837. [PubMed: 10619029]
- Herrera SC, and Bach EA (2019). JAK/STAT signaling in stem cells and regeneration: from *drosophila* to vertebrates. *Development.* 146, dev167643. [PubMed: 30696713]
- Houtz P, Bonfini A, Liu X, Revah J, Guillou A, Poidevin M, Hens K, Huang H, Deplancke B, Tsai Y, et al. (2017). Hippo, TGF- β , and Src-MAPK pathways regulate transcription of the upd3 cytokine in *Drosophila* enterocytes upon bacterial infection. *PLoS Genet.* 13, e1007091. [PubMed: 29108021]
- Houtz P, Bonfini A, Bing X, and Buchon N (2019). Recruitment of adult precursor cells underlies limited repair of the infected larval midgut in *Drosophila*. *Cell Host Microbe* 26, 412–425.e5. [PubMed: 31492656]
- Hultmark D (2003). *Drosophila* immunity: paths and patterns. *Curr. Opin. Immunol* 15, 12–19. [PubMed: 12495727]
- Hung RJ, Hu Y, Kirchner R, Liu Y, Xu C, Comjean A, Tattikota SG, Li F, Song W, Sui SH, et al. (2020). A cell atlas of the adult *Drosophila* midgut. *Proc. Natl. Acad. Sci. U S A* 117, 1514–1523. [PubMed: 31915294]
- Jiang H, Patel PH, Kohlmaier A, Grenley MO, McEwen DG, and Edgar BA (2009). Cytokine/jak/stat signaling mediates regeneration and homeostasis in the *Drosophila* midgut. *Cell* 137, 1343–1355. [PubMed: 19563763]
- Jiang H, Grenley MO, Bravo MJ, Blumhagen RZ, and Edgar BA (2011). EGFR/Ras/MAPK signaling mediates adult midgut epithelial homeostasis and regeneration in *Drosophila*. *Cell Stem Cell* 8, 84–95. [PubMed: 21167805]
- Justins L, Ripke S, Weersma RK, Duerr RH, McGovern DP, Hui KY, Lee JC, Philip Schumm L, Sharma Y, Anderson CA, et al. (2012). Hostmicrobe interactions have shaped the genetic architecture of inflammatory bowel disease. *Nature* 491, 119–124. [PubMed: 23128233]
- Kamareddine L, Robins WP, Berkey CD, Mekalanos JJ, and Watnick PI (2018). The *Drosophila* immune deficiency pathway modulates enteroendocrine function and host metabolism. *Cell Metab.* 28, 449–462.e5. [PubMed: 29937377]

- Korzelius J, Azami S, Ronnen-Oron T, Koch P, Baldauf M, Meier E, Rodriguez-Fernandez IA, Groth M, Sousa-Victor P, and Jasper H (2019). The WT1-like transcription factor Klumpfuss maintains lineage commitment of enterocyte progenitors in the *Drosophila* intestine. *Nat. Commun* 10, 4123. [PubMed: 31511511]
- Lebrun LJ, Lenaerts K, Kiers D, Pais de Barros JP, Le Guern N, Plesnik J, Thomas C, Bourgeois T, Dejong CHC, Kox M, et al. (2017). Enteroendocrine L cells sense LPS after gut barrier injury to enhance GLP-1 secretion. *Cell Rep.* 21, 1160–1168. [PubMed: 29091756]
- Lesperance DN, and Broderick NA (2020). Microbiomes as modulators of *Drosophila melanogaster* homeostasis and disease. *Curr. Opin. Insect Sci* 39, 84–90. [PubMed: 32339931]
- Liu X, Hodgson JJ, and Buchon N (2017). *Drosophila* as a model for homeostatic, antibacterial, and antiviral mechanisms in the gut. *PLoS Pathog.* 13, e1006277. [PubMed: 28472194]
- Luo L, and Wu JS (2007). A protocol for mosaic analysis with a repressible cell marker (Mosaic) in *Drosophila*. *Nat. Protoc* 1, 2583–2589.
- Marshall OJ, and Brand AH (2015). Damidseq-pipeline: an automated pipeline for processing DamID sequencing datasets. *Bioinformatics* 31, 3371–3373. [PubMed: 26112292]
- Marshall OJ, Southall TD, Cheetham SW, and Brand AH (2016). Cell-type-specific profiling of protein-DNA interactions without cell isolation using targeted DamID with next-generation sequencing. *Nat. Protoc* 11, 1586–1598. [PubMed: 27490632]
- McGovern DPB, Gardet A, Törkvist L, Goyette P, Essers J, Taylor KD, Neale BM, Ong RTH, Lagacé C, Li C, et al. (2010). Genome-wide association identifies multiple ulcerative colitis susceptibility loci. *Nat. Genet* 42, 332–337. [PubMed: 20228799]
- Meng FW, and Biteau B (2015). A Sox transcription factor is a critical regulator of adult stem cell proliferation in the *Drosophila* intestine. *Cell Rep.* 13, 906–914. [PubMed: 26565904]
- Micchelli CA, and Perrimon N (2006). Evidence that stem cells reside in the adult *Drosophila* midgut epithelium. *Nature* 439, 475–479. [PubMed: 16340959]
- Miguel-Aliaga I, Jasper H, and Lemaitre B (2018). Anatomy and physiology of the digestive tract of *Drosophila melanogaster*. *Genetics* 210, 357–396. [PubMed: 30287514]
- Miller HRP, and Nawa Y (1979). Immune regulation of intestinal goblet cell differentiation. Specific induction of nonspecific protection against helminths? *Nouv. Rev. Fr. Hematol* 21, 31–45. [PubMed: 493106]
- Von Moltke J, Ji M, Liang HE, and Locksley RM (2016). Tuft-cell-derived IL-25 regulates an intestinal ILC2-epithelial response circuit. *Nature* 529, 221–225. [PubMed: 26675736]
- Müller L, Fülöp T, and Pawelec G (2013). Immunosenescence in vertebrates and invertebrates. *Immun. Ageing* 10, 12. [PubMed: 23547999]
- Myant KB, Cammareri P, McGhee EJ, Ridgway RA, Huels DJ, Cordero JB, Schwitalla S, Kalna G, Ogg EL, Athineos D, et al. (2013). ROS production and NF- κ B activation triggered by RAC1 facilitate WNT-driven intestinal stem cell proliferation and colorectal cancer initiation. *Cell Stem Cell* 12, 761–773. [PubMed: 23665120]
- O'Brien LE, Soliman SS, Li X, and Bilder D (2011). Altered modes of stem cell division drive adaptive intestinal growth. *Cell* 147, 603–614. [PubMed: 22036568]
- Ohlstein B, and Spradling A (2007). Multipotent *Drosophila* intestinal stem cells specify daughter cell fates by differential notch signaling. *Science* 315, 988–992. [PubMed: 17303754]
- Olafsson S, McIntyre RE, Coorens T, Butler T, Jung H, Robinson PS, Lee-Six H, Sanders MA, Arestang K, Dawson C, et al. (2020). Somatic evolution in non-neoplastic IBD-affected colon. *Cell* 182, 672–684.e11. [PubMed: 32697969]
- Paredes JC, Welchman DP, Poidevin M, and Lemaitre B (2011). Negative regulation by Amidase PGRPs shapes the *Drosophila* antibacterial response and protects the Fly from innocuous infection. *Immunity* 35, 770–779. [PubMed: 22118526]
- Patel PH, Dutta D, and Edgar BA (2015). Niche appropriation by *Drosophila* intestinal stem cell tumours. *Nat. Cell Biol* 17, 1182–1192. [PubMed: 26237646]
- Peck BCE, Shanahan MT, Singh AP, and Sethupathy P (2017). Gut microbial influences on the mammalian intestinal stem cell Niche. *Stem Cells Int.* 2017, 5604727. [PubMed: 28904533]

- Petkau K, Ferguson M, Guntermann S, and Foley E (2017). Constitutive immune activity promotes tumorigenesis in *Drosophila* intestinal progenitor cells. *Cell Rep.* 20, 1784–1793. [PubMed: 28834743]
- Quevillon-Cheruel S, Leulliot N, Muniz CA, Vincent M, Gallay J, Argentini M, Cornu D, Bocard F, Lemaître B, and van Tilbeurgh H (2009). Evf, a virulence factor produced by the *Drosophila* pathogen *Erwinia carotovora*, is an S-palmitoylated protein with a newfold that binds to lipid vesicles. *J. Biol. Chem* 284, 3552–3562. [PubMed: 18978353]
- Radtke F, and Clevers H (2005). Self-renewal and cancer of the gut: two sides of a coin. *Science* 307, 1904–1909. [PubMed: 15790842]
- Reiff T, Antonello ZA, Ballesta-Illán E, Mira L, Sala S, Navarro M, Martinez LM, and Dominguez M (2019). Notch and EGFR regulate apoptosis in progenitor cells to ensure gut homeostasis in *Drosophila*. *EMBO J.* 38, e101346. [PubMed: 31566767]
- Richmond CA, Rickner H, Shah MS, Ediger T, Deary L, Zhou F, Tovaglieri A, Carlone DL, and Breault DT (2018). JAK/STAT-1 signaling is required for reserve intestinal stem cell activation during intestinal regeneration following acute inflammation. *Stem Cell Rep.* 10, 17–26.
- Round JL, and Mazmanian SK (2009). The gut microbiota shapes intestinal immune responses during health and disease. *Nat. Rev. Immunol* 9, 313–323. [PubMed: 19343057]
- Ryu JH, Kim SH, Lee HY, Bai JY, Nam YD, Bae JW, Lee DG, Shin SC, Ha EM, and Lee WJ (2008). Innate immune homeostasis by the homeobox gene caudal and commensal-gut mutualism in *Drosophila*. *Science* 319, 777–782. [PubMed: 18218863]
- Schindelin J, Arganda-Carreras I, Frise E, Kaynig V, Longair M, Pietzsch T, Preibisch S, Rueden C, Saalfeld S, Schmid B, et al. (2012). Fiji: an open-source platform for biological-image analysis. *Nat. Methods* 9, 676–682. [PubMed: 22743772]
- Southall TD, Gold KS, Egger B, Davidson CM, Caygill EE, Marshall OJ, and Brand AH (2013). Cell-type-specific profiling of gene expression and chromatin binding without cell isolation: assaying RNA pol II occupancy in neural stem cells. *Dev. Cell* 26, 101–112. [PubMed: 23792147]
- Takehana A, Yano T, Mita S, Kotani A, Oshima Y, and Kurata S (2004). Peptidoglycan recognition protein (PGRP)-LE and PGRP-LC act synergistically in *Drosophila* immunity. *EMBO J.* 23, 4690–4700. [PubMed: 15538387]
- Tian A, Wang B, and Jiang J (2017). Injury-stimulated and self-restrained BMP signaling dynamically regulates stem cell pool size during *Drosophila* midgut regeneration. *Proc. Natl. Acad. Sci. U S A* 114, E2699–E2708. [PubMed: 28289209]
- Tracy Cai X, Li H, Safyan A, Gawlik J, Pyrowolakis G, and Jasper H (2019). AWD regulates timed activation of BMP signaling in intestinal stem cells to maintain tissue homeostasis. *Nat. Commun* 10, 2988. [PubMed: 31278345]
- Troha K, Im JH, Revah J, Lazzaro BP, and Buchon N (2018). Comparative transcriptomics reveals CrebA as a novel regulator of infection tolerance in *D. melanogaster*. *PLoS Pathog.* 14, e1006847. [PubMed: 29394281]
- Troha K, Nagy P, Pivovar A, Lazzaro BP, Hartley PS, and Buchon N (2019). Nephrocytes remove microbiota-derived peptidoglycan from systemic circulation to maintain immune homeostasis. *Immunity* 51, 625–637.e3. [PubMed: 31564469]
- Ye L, Bae M, Cassilly CD, Jabba SV, Thorpe DW, Martin AM, Lu HY, Wang J, Thompson JD, Lickwar CR, et al. (2021). Enteroendocrine cells sense bacterial tryptophan catabolites to activate enteric and vagal neuronal pathways. *Cell Host Microbe* 29, 179–196.e9. [PubMed: 33352109]
- Yu HH, Chen CH, Shi L, Huang Y, and Lee T (2009). Twin-spot MARCM to reveal the developmental origin and identity of neurons. *Nat. Neurosci* 12, 947–953. [PubMed: 19525942]
- Zeng X, and Hou SX (2015). Enteroendocrine cells are generated from stem cells through a distinct progenitor in the adult *drosophila* posterior midgut. *Development* 142, 644–653. [PubMed: 25670791]
- Zeng X, Chauhan C, and Hou SX (2010). Characterization of midgut stem cell- and enteroblast-specific Gal4 lines in *drosophila*. *Genesis* 48, 607–611. [PubMed: 20681020]
- Zhai Z, Kondo S, Ha N, Boquete JP, Brunner M, Ueda R, and Lemaitre B (2015). Accumulation of differentiating intestinal stem cell progenies drives tumorigenesis. *Nat. Commun* 6, 10219. [PubMed: 26690827]

- Zhai Z, Boquete JP, and Lemaitre B (2017). A genetic framework controlling the differentiation of intestinal stem cells during regeneration in *Drosophila*. *PLoS Genet.* 13, e1006854. [PubMed: 28662029]
- Zhou J, Florescu S, Boettcher AL, Luo L, Dutta D, Kerr G, Cai Y, Edgar BA, and Boutros M (2015). Dpp/Gbb signaling is required for normal intestinal regeneration during infection. *Dev. Biol* 399, 189–203. [PubMed: 25553980]

Author Manuscript

Author Manuscript

Author Manuscript

Author Manuscript

Highlights

- Indigenous and pathogenic microbes promote opposite changes to gut epithelial structure
- Microbes regulate ISC differentiation and determine gut epithelium cell composition
- Microbe-dependent activation of immune pathways regulates ISC differentiation
- The balance of Imd-Relish and JAK-STAT pathway activity governs ISC differentiation

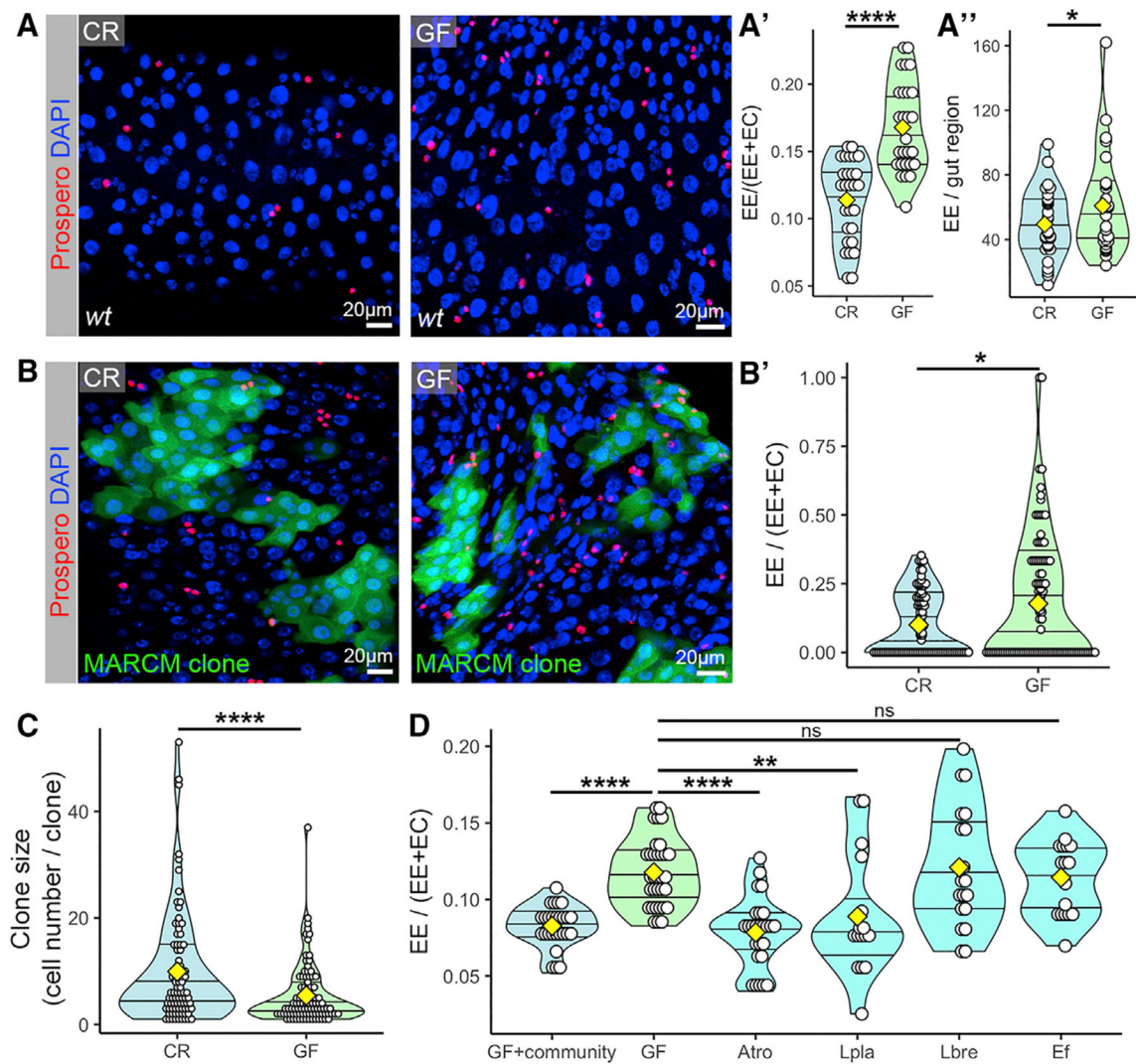


Figure 1. Microbiota regulates the proportion of EEs in the midgut epithelium

(A–A'') The ratio of Prospero-labeled EEs to total differentiated cell types ($EE/(EE+EC)$)

(A') and total number of EEs (A'') are higher in germ-free (GF) flies compared with conventionally reared (CR) animals.

(B–B') Clonal analysis of ISC fate revealed increased proportion of EEs in GF animals compared with CR animals 10 days post clone induction. The number of Prospero⁺ EEs and ECs in every clone was counted, and the ratio of $EE/(EE+EC)$ was plotted.

(C) Clone size reflecting the total number of cells per each clone islet is smaller in GF intestines.

(D) Elevated epithelial density of EEs is reverted after reassociation of GF animals with microbiota (GF + community) or certain single bacteria (*Acetobacter tropicalis* [Atr] or *Lactobacillus plantarum* [Lpla]) but remains unchanged when reassociated with *Lactobacillus brevis* [Lbre] or *Enterococcus faecalis* [Ef].

Statistical significance: mean values of at least 3 biological repeats are represented, * $p < 0.05$, ** $p < 0.01$, **** $p < 0.0001$.

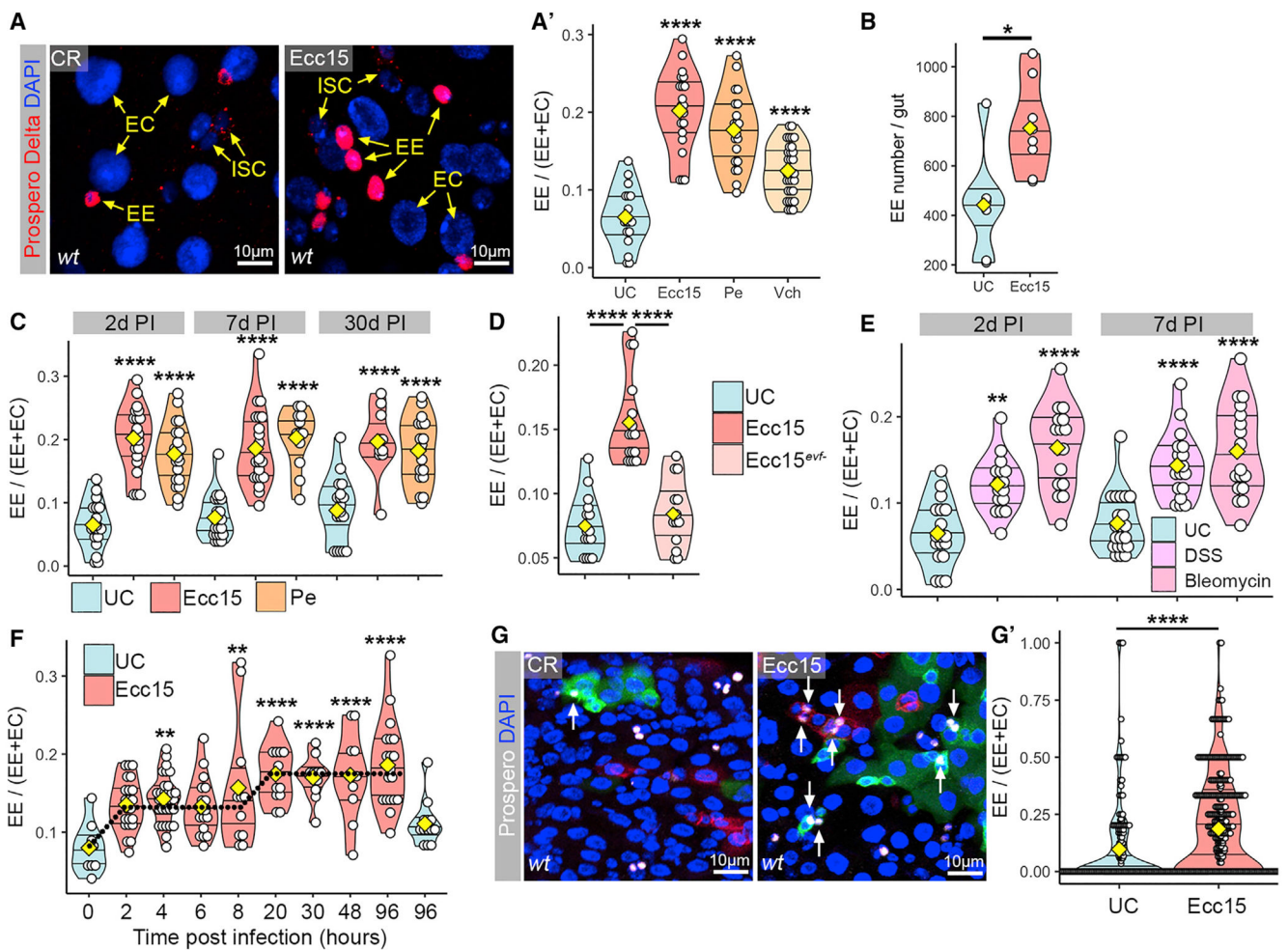


Figure 2. Pathogenic microbes increase the production of EEs

(A–A') Oral ingestion of pathogenic *Erwinia carotovora ssp. carotovora 15* (*Ecc15*), *Pseudomonas entomophila* (*Pe*), or the human enteropathogen *Vibrio cholerae* (*Vch*) promotes increased formation of Prospero⁺ EEs compared with unchallenged (UC) as seen with the increase in EE/(EE+EC).

(B) Total number of Prospero⁺ EEs increased upon *Ecc15* infection.

(C) High proportion of EEs remained unchanged over a 30-day time period in response to *Ecc15* or *Pe* infection.

(D) Infection with an avirulent *Ecc15*^{evf-} mutant bacteria does not increase the proportion of EEs.

(E) Abiotic stress induced by ingestion of dextran sodium sulfate (DSS) or bleomycin results in the increase of Prospero⁺ EE density.

(F) Changes in epithelial cell composition in response to *Ecc15* infection occur in two discrete steps: first, the proportion of EEs increases slightly due to massive EC delamination between 2 and 8 h post *Ecc15* infection; second, infection-induced compensatory ISC proliferation results in the *de novo* production of EEs 20 h post infection.

(G–G') Clonal analysis after pathogenic infection reveals that EEs (white arrows) are generated at higher rate in response to *Ecc15*.

Statistical significance: mean values of at least 3 biological repeats are represented, * $p < 0.05$, ** $p < 0.01$, **** $p < 0.0001$.

Author Manuscript

Author Manuscript

Author Manuscript

Author Manuscript

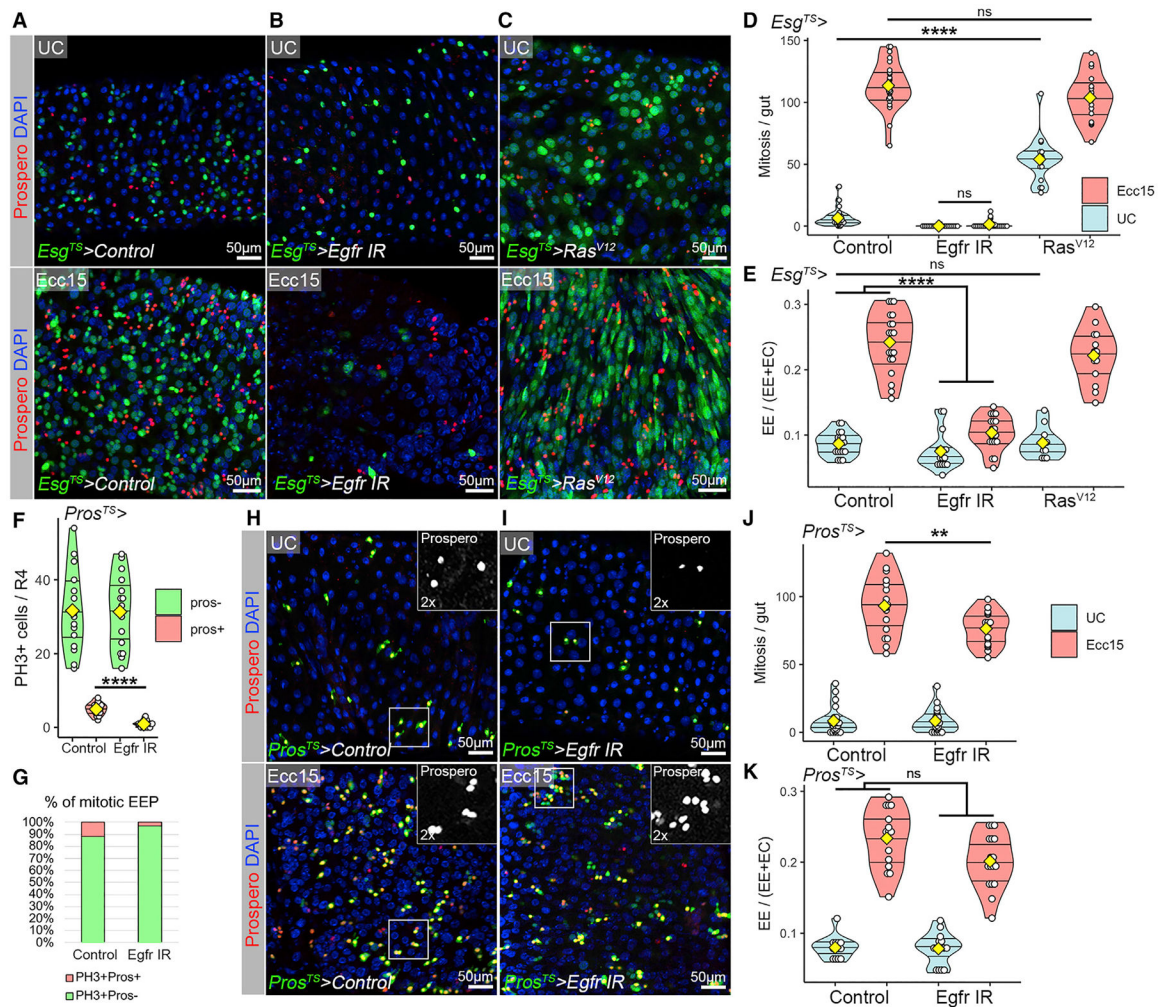


Figure 3. Changes in ISC differentiation underlie the increase in EEs upon infection

(A–E) Infection with *Ecc15* triggers compensatory ISC proliferation (D) and increases the density of Prospero⁺ EEs (A and E). *Esgargot*-specific knockdown of Egfr signaling by *Egfr-IR* decreases infection-triggered ISC proliferation (D) and dampens EE accumulation (B and E). *Esgargot*-specific activation of Egfr signaling by expressing constitutively active *Ras^{V12}* results in ISC hyperproliferation (D) but has no effect on EE density in UC midguts or in response to *Ecc15* infection (C and E).

(F–K) Blocking Egfr signaling by *Prospero-Gal4^{TS}* diminishes only EEP mitosis as reported by the decrease of PH3⁺Prospero⁺ cell numbers (F and G). Blockage of EEP mitosis has a minor effect on *Ecc15* infection induced ISC proliferation (J) and does not change increased EE density in response to *Ecc15* infection (H, I, and K). Insets show the presence of Prospero⁺ cell doublets in *Ecc15* control and after *Egfr-IR* (H and I).

Statistical significance: mean values of at least 3 biological repeats are represented, **p < 0.01, ****p < 0.0001.

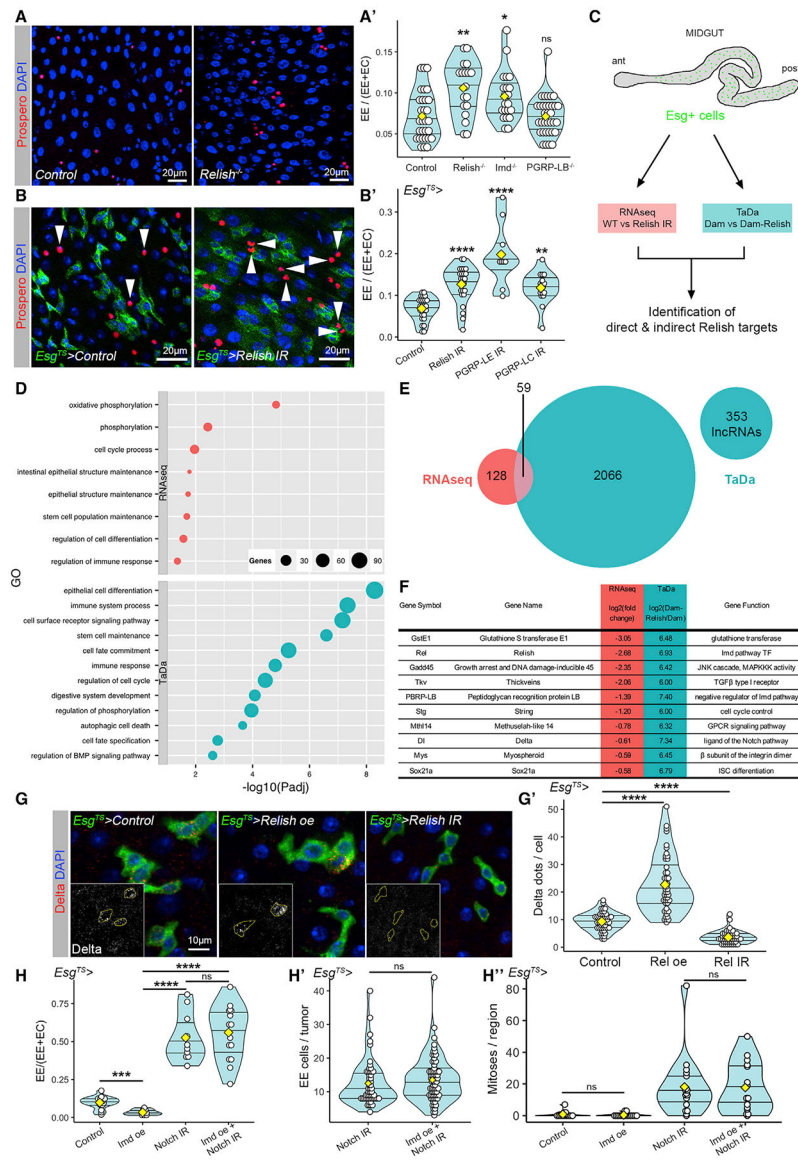


Figure 4. Imd-Relish pathway promotes EC fate via directly regulating pro-EC differentiation factors

(A–A') Epithelial cell composition is changed in *Rel^{-/-}* and *Imd^{-/-}* mutants. We detected a higher proportion of Prospero⁺ EEs over ECs in these mutants, but it remained unchanged in *PGRP-LB^{-/-}* animals.

(B–B') *Esg*ot-specific depletion of *Relish*, *PGRP-LE*, and *PGRP-LC* increased EE density (white arrowheads mark Prospero⁺ EEs in B).

(C) Workflow for progenitor-specific Relish target gene identification.

(D) Gene Ontology (GO) categories representing group of genes downregulated in progenitors after *Relish IR* and bound by *Dam-Relish* in *Esg*ot⁺ progenitor cells.

(E and F) Group (D) of genes that are downregulated in progenitors after *Relish IR* and bound by *Dam-Relish* are involved in various cellular processes (F).

(G–G') *Relish* is sufficient and required for the regulation of *Notch* receptor ligand *Delta* in ISCs (yellow dashed lines mark Delta⁺ cells in F).

(H–H⁺) *Escargot*-specific overexpression of *imd* decreases EE proportion in the midgut and has no effect on *Notch*-depletion-mediated Prospero⁺ EE accumulation, EE numbers in tumors, and mitoses.

Statistical significance: mean values of at least 3 biological repeats are represented, *p < 0.05, **p < 0.01, ***p < 0.001, ****p < 0.0001.

Author Manuscript

Author Manuscript

Author Manuscript

Author Manuscript

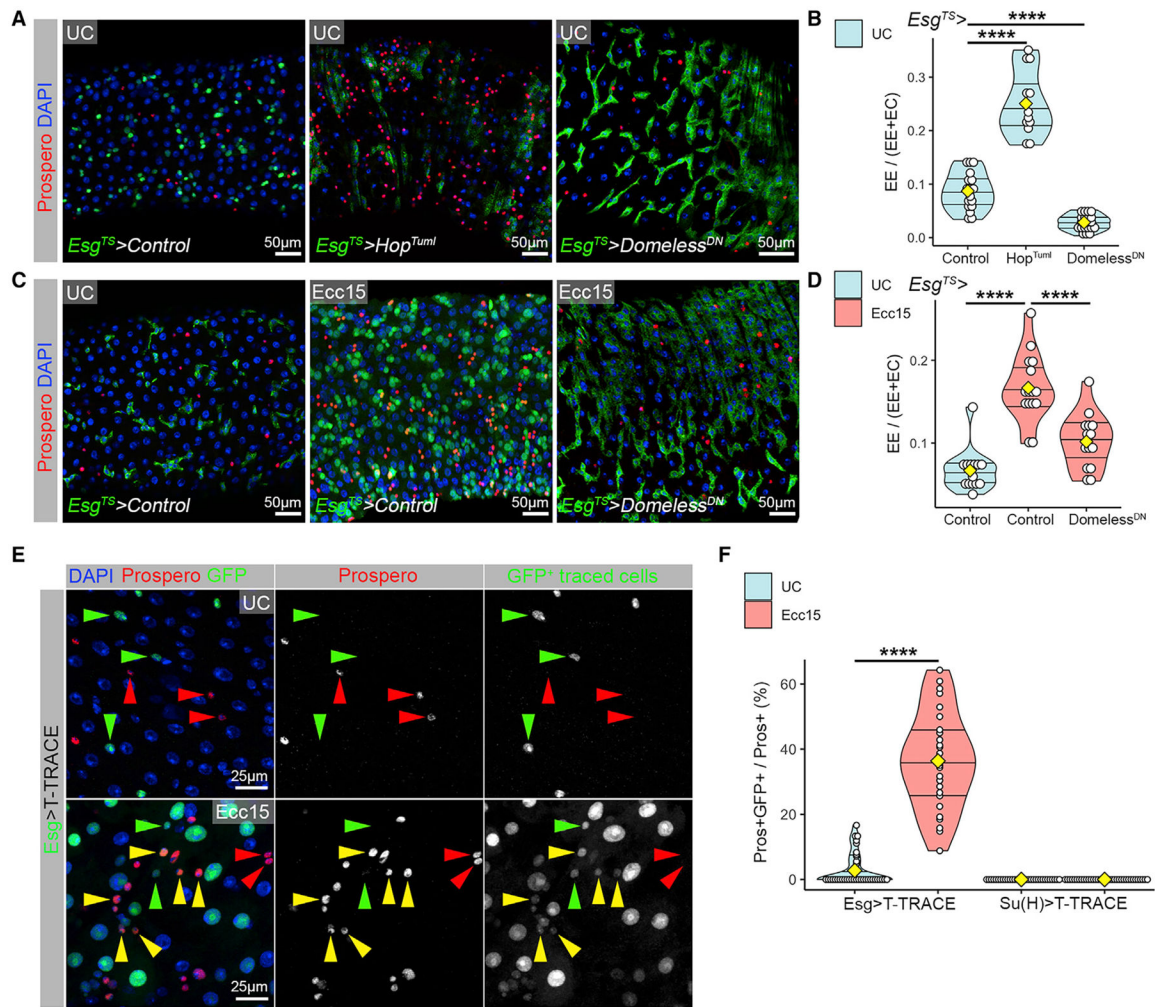


Figure 5. ISC-specific JAK-STAT activation promotes infection-triggered *de novo* production of EEs

(A and B) Ectopic activation or blockage of JAK-STAT signaling by expressing *Hop^{Tum1}* or *Domeless^{DN}* in *Escargot⁺* progenitors is sufficient to increase or decrease EE density, respectively.

(C and D) *Escargot*-specific blockage of JAK-STAT signaling by *Domeless^{DN}* suppresses the gain of Prospero⁺ EEs in response to *Ecc15* infection.

(E and F) Lineage-tracing experiments by using *Escargot*>T-TRACE and *Su(H)*>T-TRACE reveal that *Ecc15*-infection-triggered *de novo*-produced Prospero⁺ (yellow arrowheads) EEs are exclusively ISC daughter cells. Green arrowheads label ISCs and EBs, while red arrowheads show Prospero⁺ EEs. Graph represents the proportional increase of GFP-labelled Prospero⁺ EEs over total EEs in response to *Ecc15* infection found only upon tracing *Escargot⁺* cells.

Statistical significance: mean values of at least 3 biological repeats are represented, *****p* < 0.0001.

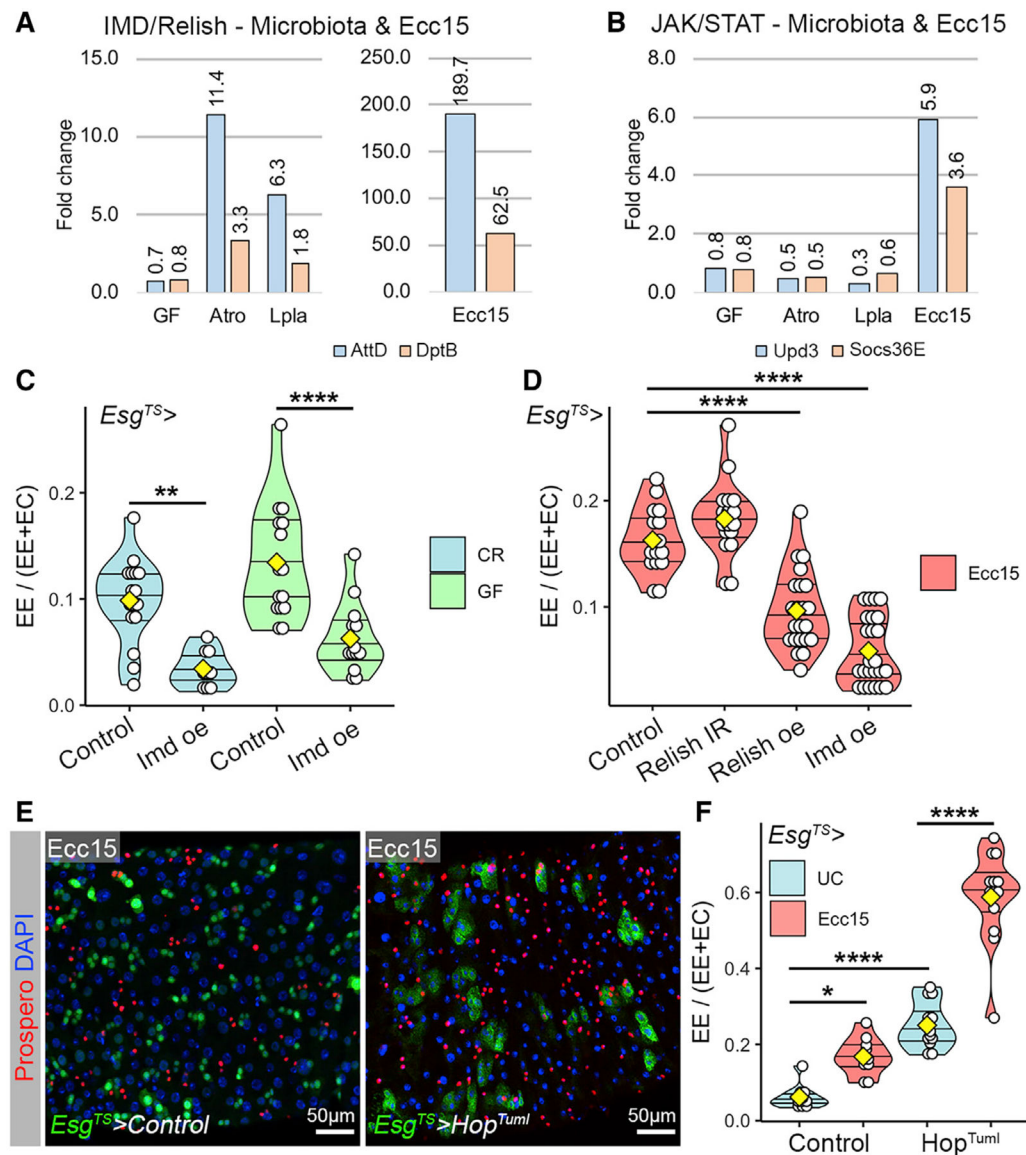


Figure 6. The balance between Imd-Relish and JAK-STAT pathways determines the influence of microbes on ISC differentiation

(A and B) Activity of Imd-Relish (A) and JAK-STAT

(B) pathways as reported by target gene (AttacinD [AttD] and DipterinB [DptB] for Imd-Relish and Suppressor of cytokine signaling at 36E [Socs36E] for JAK-STAT) or activating ligand (Unpaired3 [Upd3] for JAK-STAT) expression is low in the midgut of GF flies compared with CR counterparts. Oral ingestion of high-dose *Atro* or *Lpla* by GF flies triggers the Imd-Relish pathway but not JAK-STAT signaling, while *Ecc15* induces both.

(C) *Escargot*-specific *imd* overexpression results in a decline in EE density both in CR and GF animals.

(D) *Escargot*-specific depletion of *Relish* has no effect on *Ecc15*-induced EE accumulation, while *relish* and *imd* overexpression suppress EE gain in response to *Ecc15* infection.

(E and F) *Escargot*-specific activation of JAK-STAT signaling by *Hop^{Tuml}* highly increases EE density both in UC and *Ecc15*-infected flies.

Statistical significance: mean values of at least 3 biological repeats are represented, * $p < 0.05$, ** $p < 0.01$, **** $p < 0.0001$.

Author Manuscript

Author Manuscript

Author Manuscript

Author Manuscript

KEY RESOURCES TABLE

REAGENT or RESOURCE	SOURCE	IDENTIFIER
Antibodies		
mouse anti-Prospero	DSHB	MR1A, RRID: AB_528440
mouse anti-Delta	DSHB	C594.9B, RRID: AB_528194
chicken anti-GFP	Thermo Fisher	A10262, RRID: AB_2534023
rabbit anti-Relish	RayBiotech	ABIN1111036, RRID: AB_11219024
rabbit anti-Sox21a and rabbit anti-PH3	Benoit Biteau	Meng and Biteau, 2015
donkey anti-mouse-555	EMD Millipore	06-570, RRID: AB_310177
donkey anti-rabbit-555	Thermo Fisher	A31570, RRID: AB_2536180
donkey anti-mouse-647	Thermo Fisher	A31572, RRID: AB_162543
donkey anti-rabbit-647	Thermo Fisher	A31571, RRID: AB_162542
goat anti-chicken-488	Thermo Fisher	A31573, RRID: AB_2536183
goat anti-chicken-488	Thermo Fisher	A11039, RRID: AB_142924
Bacterial and virus strains		
<i>Erwinia carotovora</i> ssp. <i>carotovora</i> 15	This strain is available upon request	N/A
<i>Pseudomonas entomophila</i>	This strain is available upon request	N/A
<i>Vibrio cholerae</i>	This strain is available upon request	N/A
<i>Acetobacter tropicalis</i>	This strain is available upon request	N/A
<i>Lactobacillus plantarum</i>	This strain is available upon request	N/A
Chemicals, peptides, and recombinant proteins		
DAPI	Sigma-Aldrich	D9564
Alexa Fluor 555 Phalloidin	Thermo Fisher	R415
Citifluor AF1	EMS	17970-100
Elastase	Sigma-Aldrich	E0258
DSS	EMD Millipore	80502-348
Bleomycin	Enzo Life Sciences	89156-580
20% paraformaldehyde	EMS	15713
Grape agar powder	Flystuff	47-102
Trizol	Life Technologies	15596018
Critical commercial assays		
RNeasy Mini kit	Qiagen	74106
Quantseq 3' mRNA-Seq	Lexogen	015.24
qScript cDNA Synthesis Kit	Quanta	95150-01K

REAGENT or RESOURCE	SOURCE	IDENTIFIER
PerfeCTa SYBR Green FastMix	Quanta	95047-100
DNeasy Blood and Tissue kit	Qiagen	69506
Deposited data		
DamID	this paper	SRA: PRJNA736303
RNAseq	this paper	SRA: PRJNA757772 SRA: PRJNA779708
Experimental models: Organisms/strains		
Hikone-A-W	Bloomington Drosophila Stock Center	#4
Oregon-R-P2	Bloomington Drosophila Stock Center	#2376
DGRP-391	Bloomington Drosophila Stock Center	#25191
DGRP-859	Bloomington Drosophila Stock Center	#25210
Rel ^{E20}	Hedengren et al., 1999	N/A
ImdR ¹⁵⁶	Hedengren et al., 1999	N/A
PGRP-LE ¹¹² /LC ^{E12}	Takehana et al., 2004	N/A
PGRP-LB KO	Paredes et al., 2011	N/A
tub-Gal80 ^{TS} ; Da-Gal4	Bloomington Drosophila Stock Center	#86326
Esg-Gal4/CyOlacZ; UAS-GFP, tub-Gal80 ^{TS}	Jiang et al., 2009	N/A
Su(H)GBE-Gal4; UAS-GFP, tub-Gal80 ^{TS}	Jiang et al., 2009	N/A
UAS-GFP, tub-Gal80 ^{TS} ; prosv1-Gal4 / TM6B	Zeng et al., 2010	N/A
UAS-Imd	Georgel et al., 2001	N/A
UAS-Rel	Georgel et al., 2001	N/A
UAS-RasV12	Bloomington Drosophila Stock Center	#4847
UAS-Dome-DN	Harrison et al., 1995	N/A
UAS-Hop ^{Tum1}	Harrison et al., 1995	N/A
UAS-nls-GFP	Bloomington Drosophila Stock Center	#4775
TI{2A-GAL4}AstC[2A-GAL4]	Bloomington Drosophila Stock Center	#84595
TI{2A-GAL4}Tk[2A-GAL4]	Bloomington Drosophila Stock Center	#84693
UAS-Rel-IR	Bloomington Drosophila Stock Center	#33661, #28943
UAS-PGRP-LE-IR	Bloomington Drosophila Stock Center	#60038
UAS-PGRP-LC-IR	Bloomington Drosophila Stock Center	#33383
UAS-Notch-IR	Bloomington Drosophila Stock Center	#33611
UAS-EGFR-IR	Bloomington Drosophila Stock Center	#25781
Esg-Gal4,Ubi-p63e-loxP-stop-loxp-GFP	Zeng and Hou, 2015	N/A
Su(H)GBE-Gal4,Ubi-p63e-loxP-stop-loxp-GFP	Zeng and Hou, 2015	N/A

REAGENT or RESOURCE	SOURCE	IDENTIFIER
UAS-RedStinger, UAS-FLP, Ubi-p63(FRT.STOP)Stinger	Bloomington Drosophila Stock Center	#28280
yw; FRT40A UAS CD8 RFT, UAS CD2-Mir / CyO; tubGal4, tubgal80ts / TM6C	Yu et al., 2009	N/A
hsflp; FRT40A UAS CD2 RFT, UAS GFP-Mir/CyO	Yu et al., 2009	N/A
Oligonucleotides		
Fw primer (Dam-Rel cloning): GCGGCCGCGGATGAACATGAATCAGTACTACG	this paper	N/A
Rv primer (Dam-Rel cloning): CGGCCGAGTCAAGTTGGGTTAACCAGTAG	this paper	N/A
Dpt Fw: GCTGCGCAATCGCTTCTACT	(Troha et al., 2019)	N/A
Dpt Rv: TGGTGGAGTGGGCTTCATG	(Troha et al., 2019)	N/A
Rpl32 Fw: GACGCTCAAGGGACAGTATCTG	(Troha et al., 2019)	N/A
Rpl32 Rv: AAACGCGTTCTGCATGAG	(Troha et al., 2019)	N/A
Software and algorithms		
R Studio	RStudio Team (2020)	N/A
Adobe Photoshop (23.1.1)	Adobe	N/A
Integrative Genomics Viewer (V2.5.3)		N/A
ImageJ	NIH	N/A